Postprint of: Malikan, M., Electro-thermal buckling of elastically supported double-layered piezoelectric nanoplates affected by an external electric voltage, Multidiscipline Modeling in Materials and Structures, Vol. 15, No. 1 (2019), pp. 50-78. https://doi.org/10.1108/MMMS-01-2018-0010

Electro-thermal buckling of elastically supported double-layered piezoelectric nanoplates affected by an external electric voltage

Abstract

This paper aims to present the electro-thermal buckling of double-layered piezoelectric nanoplates (DLPNs) using modified couple stress theory. DLPNs are subjected to a uniform temperature which developed from a thermal environment and an external electric voltage (EEV) is applied on the plates. Due to the existing thermal buckling analysis in which thermal stress resultants depend on the thickness only; therefore, a comprehensive method by considering thermal stresses at both length and width of the plate is investigated. A simplified four-variable shear deformation plate theory is employed and the governing differential equations are obtained using the variational formulation. Modified couple stress theory is applied in order to consider size-dependent effects. Because the presented temperature distribution method is relatively new particularly in nanostructures and there has never been similar studying, so, in order to compare the results, a validation is done with the results of graphene sheets. Results are presented by change in some parameters such as aspect ratio, effects of boundary conditions and influence of the length scale parameter on the thermal stability of DLPNs.

Keywords: Electro-thermal buckling; Double-layered piezoelectric nanoplates; External electric voltage; Modified couple stress theory; Simplified four-variable shear deformation plate theory

1. Introduction

Piezoelectricity effect has been defined as a linear-electromechanical reaction between both electrical and mechanical states in adiabatic materials and crystals which do not have central symmetry. Indeed, piezoelectric is a material in which electrical field is created under mechanical pressures or stresses. This phenomenon is called direct piezoelectric effect which is a returnable process. Reversely, whenever a material with such a property is embedded in the electric field, the mechanical deformation will occur (reverse piezoelectric effect) [1]. By the help of piezoelectric nanomaterials, the minute produced waste oscillating energies in the noises environment, power of wind and the movement of water or waves can be collected and used as propulsion for directly water decomposition and producing of energy. Currently, the major limitation of such advanced materials is their use in the nanoscale devices. Scientists are cutting, fragmenting and grinding these materials in order to use them in nanodevices; however, the operations have low precision and are done as a trial and error method [2].

Due to the importance of mechanical behavior forecast of piezoelectric nanomaterials and according to difficulties in the use of experimental methods as well as the high cost for analyzing in the laboratory, so, it can be highly

recommended to use the theoretical methods for investigating nanoscale materials. Therefore, many kinds of research have been presented over the past years for prediction of the mechanical behavior of nanomaterials which are briefly shown by the following studies. Ke et al. investigated the nonlinear vibration [3] and post-buckling [4] behaviors of nonlocal Timoshenko piezoelectric nanobeams under combined thermo-electro-mechanical loadings. Vibration and buckling analysis of a piezoelectric nanoplate considering surface effects and in-plane constraints have been presented by Jiang and Yan [5]. Free vibration analysis for single-layered graphene sheets in an elastic matrix via modified couple stress theory was studied by Civalek and Akgöz [6]. They used classical plate theory and analytical Fourier series approach in the research. Results presented that the effect of the material length scale parameter is more significant for higher modes of vibration. Dai et al. [7] investigated buckling analysis of a piezoelectric viscoelastic nanobeam subjected to van der Waals forces. Wang et al. [8] examined the nonlinear pull-in instability and free vibration of micro/nanoscale plates with surface energy using a modified couple stress model. Their results showed that the effect of the surface energy and the material length scale decreased if the size of the plate increased. Shariati et al. [9] studied post-buckling of functionally graded nanobeams based on modified couple stress theory under general beam theory. The obtained results indicate that the first-order beam theory has some errors in estimating the amplitude of buckling. He et al. [10] analyzed buckling and post-buckling analyses of piezoelectric hybrid microplates subject to thermo-electro-mechanical loads based on the modified couple stress theory. They used first-order shear deformation theory for deriving governing equations and applied Galerkin method in order to solve the equilibrium equations. Malikan et al. [11] published buckling of double-layered nanoplates under shear and thermal loads based on the elastic matrix using differential quadrature method. Moharam and Alireza Habibnejad Korayem [12] studied modeling of atomic force microscope (AFM) with a piezoelectric layer based on the modified couple stress theory with geometric discontinuities. Pan et al. [13] extended free vibration of three-dimensional anisotropic layered composite nanoplates based on modified couple stress theory. Their results revealed that the material length scale has a much larger effect on the natural frequencies in the thin plate than those in thick plate. Malikan [14] presented electro-mechanical shear buckling of a piezoelectric nanoplate using modified couple stress theory based on a simplified first-order shear deformation theory. The results showed that the effect of external electric voltage on the critical shear load occurring on the piezoelectric nanoplate is insignificant.

Size effect is a subject of current increasing interest due to the fact that current applications in modern technology involve a variety of length scales ranging from a few centimeters down to a few nanometers [15]. Structural materials display a strong size-dependence when deformed non-uniformly into the inelastic range: smaller is stronger. This effect has important implications for an increasing number of applications in structural failure, electronics, functional coatings, composites, micro-electro-mechanical systems (MEMS), nanostructured materials, micro/nanometer fabrication technologies, etc. The mechanical behavior of these applications cannot be characterized by classical continuum theories because they incorporate no ‘material length scales’ and consequently predict no size effects. On the other hand, it is still not possible to perform quantum and atomistic simulations on realistic time and structures. It was therefore necessary to develop a scale-dependent continuum theory bridging the gap between the classical continuum theories and the atomistic simulations in order to be able to design the size-dependent structures of modern technology [15]. Modified couple stress theory is applied in this work for this purpose, in which a material length scale is implicitly and explicitly introduced into the governing equations. It is worth noting that the couple

stress theories are forms of strain gradient theories by taking the first strain gradient parameter of Mindlin [16]. In couple stress theory the potential energy-density is assumed to be a function of the strain and the curl of the strain instead of the strain alone [17-19].

This paper investigates double-layered piezoelectric nanoplates in a thermal environment in order to consider temperature effects on such materials. Regarding existing thermal buckling of nanoplates, we have seen thermal stresses differential along the thickness of nanoplates in order to obtain critical buckling temperature. As a matter of fact, there has never been any considering about presence of thermal stresses based on the nanoplate's dimensions dependency and thermal stress resultants are only a function of thickness, which in fact, cannot be comprehensive. So, current research studies thermal buckling analysis with investigating thermal stresses based on the thickness as well as length and width of the plate. On the other hand, finding a thermal function which shows heat transfer in nanomaterials among atoms is so difficult, and it has not already derived. Therefore, a thermal function which was derived for macro materials is employed. In order to obtain governing equations, the nonlinear strains of Von-Kármán have been considered. In addition, the small-scale effects are studied with utilizing modified couple stress theory. Moreover, Galerkin analytical solution is used to solve the stability equations in various boundary conditions. Finally, the effects of different parameters such as; changes in the length scale parameter, aspect ratio, and boundary effects of edges in various conditions under thermal stresses have been evaluated.

2. Governing equations

A double-layered rectangular piezoelectric nanosize plate is assumed as Fig. 1 in the thermal environment under an external electric voltage. The plate is embedded in a two-parameter Winkler-Pasternak elastic foundation thoroughly in the linear form. Also, van der Waals forces are assumed to be linear spring interlayers. For terminology of the plate sizes, L_x and L_y are used for presenting length and width of the nanoplates respectively, and h has shown the thickness of either of the nanoplates.

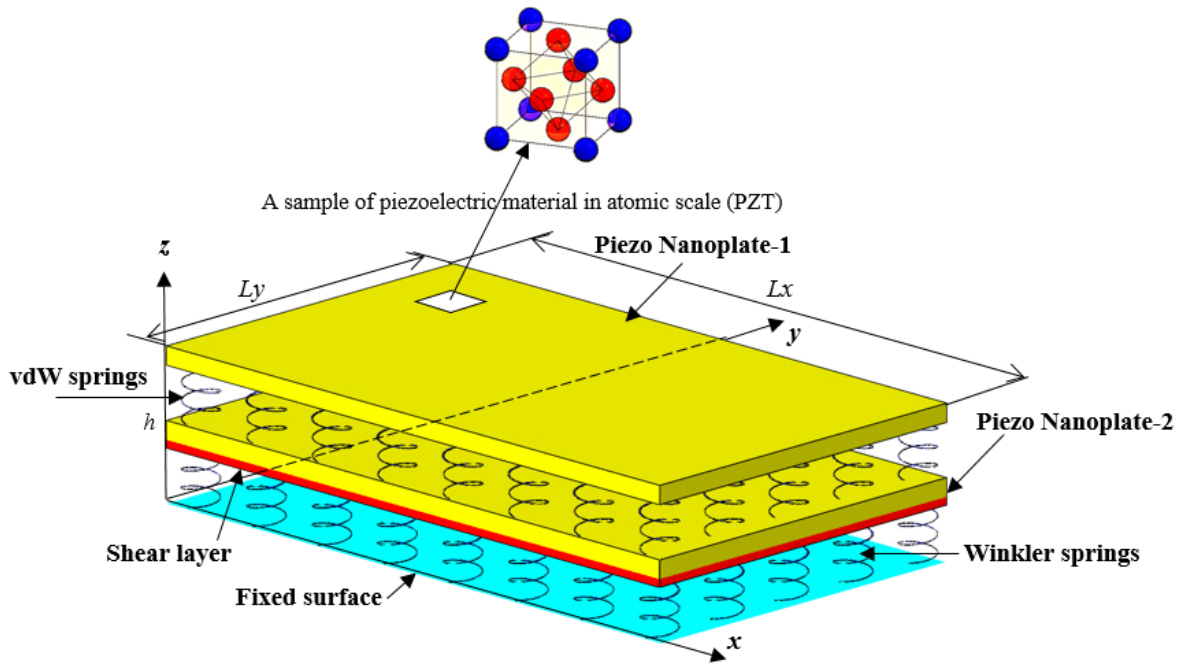

Fig. 1. Schematic figure of rectangular double-layered piezoelectric nanoplates on the Winkler-Pasternak matrix

Not to mention that a complete plate theory cannot be easily found and compulsorily the current theories should be refined. Even though, over the past two decades, many researchers have studied the mechanical behavior of the nanostructures based on the first-order shear deformation theory (FSDT) which has the more accurate results than classical one. It should be noted that the FSDT has some considerable assumptions. For example, in the theory, the shear stress distribution will be invariable during deformation along the thickness of the plate. This assumption can no longer be true when the remarkable thickness to length ratio will be considered because transverse shear stress is significant in such a plate and should be presented in its actual distribution. In the paper, FSDT has been refined and simplified in a different form in order to remove minor errors in the contractual theory. Therefore, in this paper, the governing equations are derived based on the simplified first-order shear deformation theory (S-SFDT) [14]. Considering the S-FSDT, the displacement field can be presented as:

$$\begin{Bmatrix} U(x,y,z) \\ V(x,y,z) \\ W(x,y,z) \end{Bmatrix} = \begin{Bmatrix} u(x,y) - z\dfrac{\partial w_b(x,y)}{\partial x} \\ v(x,y) - z\dfrac{\partial w_b(x,y)}{\partial y} \\ w_b(x,y) + w_s(x,y) \end{Bmatrix} \tag{1a-c}$$

where w_b denotes bending component of deflection and the shear component is defined with w_s. Also, u and v are the displacement components along x and y-axis, z is a variable related to thickness of the plate.

All continuum theories used these days have been presented for considering size-dependent influences [17, 19-20]. Recently, the modified couple stress theory [21-22] has been applied in which a length scale parameter has been used to calculate the effect of small-scale. According to this higher-order continuum theory and using Hamilton's principle, the governing equations of a rectangular piezoelectric nanoplate will be derived. Hence, the equations of the total potential energy (V) are expressed as:

$$V = S + \Omega \tag{2}$$

In which S and Ω are strain energy and work done by external loads, respectively. The virtual strain energy can be calculated as:

$$\delta S = \iiint_v \left(\sigma_{ij}\delta\varepsilon_{ij} + m_{ij}\delta\chi_{ij} - D_k\delta E_k\right)dV = \iiint_v \left[\left(\sigma_{ij}^T + \sigma_{ij}^m\right)\delta\varepsilon_{ij}^{total} + m_{ij}\delta\chi_{ij} - D_k\delta E_k\right]dV = 0 \tag{3}$$

where σ_{ij}^T, σ_{ij}^m, ε_{ij}, m_{ij}, χ_{ij}, D_k, and E_k are thermal stress tensor, mechanical stress tensor, Lagrangian strain tensor, deviatoric part of the couple stress tensor, symmetric curvature tensor, electric displacement and electric field vectors, respectively [3, 23-28]. Then, the stress and electric fields are:

$$\sigma_{ij} = C_{ijkl}\varepsilon_{kl} - e_{kij}E_k\,,\quad D_i = e_{ikl}\varepsilon_{kl} + \kappa_{ij}E_k \tag{4a-b}$$

In which C_{ijkl} is stiffness matrix of the material, e_{ikl} and κ_{ij} are piezoelectric and dielectric quantities respectively, which should be defined as:

$$e_{kij} = \begin{bmatrix} 0 & 0 & \bar{e}_{31} \\ 0 & 0 & \bar{e}_{31} \\ \bar{e}_{15} & 0 & 0 \\ 0 & \bar{e}_{15} & 0 \\ 0 & 0 & 0 \end{bmatrix},\ e_{ikl} = e_{kij}^T,\ \kappa_{ij} = \begin{bmatrix} \bar{\kappa}_{11} & 0 & 0 \\ 0 & \bar{\kappa}_{11} & 0 \\ 0 & 0 & \bar{\kappa}_{33} \end{bmatrix} \tag{5a-c}$$

The Lagrangian strain tensor will be expressed as follows:

$$\varepsilon_{ij}=\frac{1}{2}\left(\frac{\partial u_i}{\partial x_j}+\frac{\partial u_j}{\partial x_i}+\frac{\partial u_k}{\partial x_i}\frac{\partial u_k}{\partial x_j}\right);\ i,j,k=1,2,3 \tag{6}$$

$$\begin{Bmatrix}\varepsilon_{xx}\\ \varepsilon_{yy}\\ \gamma_{xz}\\ \gamma_{yz}\\ \gamma_{xy}\end{Bmatrix}=\begin{Bmatrix}\dfrac{\partial u}{\partial x}-z\dfrac{\partial^2 w_b}{\partial x^2}+\dfrac{1}{2}\left(\dfrac{\partial w_b}{\partial x}\right)^2+\dfrac{1}{2}\left(\dfrac{\partial w_s}{\partial x}\right)^2+\dfrac{\partial w_b}{\partial x}\dfrac{\partial w_s}{\partial x}\\ \dfrac{\partial v}{\partial y}-z\dfrac{\partial^2 w_b}{\partial y^2}+\dfrac{1}{2}\left(\dfrac{\partial w_b}{\partial y}\right)^2+\dfrac{1}{2}\left(\dfrac{\partial w_s}{\partial y}\right)^2+\dfrac{\partial w_b}{\partial y}\dfrac{\partial w_s}{\partial y}\\ \dfrac{\partial w_s}{\partial x}\\ \dfrac{\partial w_s}{\partial y}\\ \left(\dfrac{\partial u}{\partial y}+\dfrac{\partial v}{\partial x}\right)-2z\dfrac{\partial^2 w_b}{\partial x\partial y}+\left(\dfrac{\partial w_b}{\partial x}+\dfrac{\partial w_s}{\partial x}\right)\left(\dfrac{\partial w_b}{\partial y}+\dfrac{\partial w_s}{\partial y}\right)\end{Bmatrix} \tag{7a-e}$$

And symmetric curvature tensor (χ_{ij}) and also couple stress quantity (m_{ij}) can be defined in the following equations:

$$\chi_{ij}=\frac{1}{2}\left(\frac{\partial \theta_i}{\partial x_j}+\frac{\partial \theta_j}{\partial x_i}\right),\ i,j=1,2,3,\ \theta=\frac{1}{2}Curl\left(u\right) \tag{8a-b}$$

$$\begin{Bmatrix}\chi_x\\ \chi_y\\ \chi_{xy}\\ \chi_{xz}\\ \chi_{yz}\end{Bmatrix}=\begin{Bmatrix}\dfrac{1}{2}\left(2\dfrac{\partial^2 w_b}{\partial x\partial y}+\dfrac{\partial^2 w_s}{\partial x\partial y}\right)\\ \dfrac{1}{2}\left(-2\dfrac{\partial^2 w_b}{\partial x\partial y}-\dfrac{\partial^2 w_s}{\partial x\partial y}\right)\\ \dfrac{1}{4}\left(-2\dfrac{\partial^2 w_b}{\partial x^2}+2\dfrac{\partial^2 w_b}{\partial y^2}-\dfrac{\partial^2 w_s}{\partial x^2}+\dfrac{\partial^2 w_s}{\partial y^2}\right)\\ \dfrac{1}{4}\left(\dfrac{\partial^2 v}{\partial x^2}-\dfrac{\partial^2 u}{\partial x\partial y}\right)\\ \dfrac{1}{4}\left(-\dfrac{\partial^2 u}{\partial y^2}+\dfrac{\partial^2 v}{\partial x\partial y}\right)\end{Bmatrix} \tag{9a-e}$$

$$m_{ij}=2G_{xy}l^2\chi_{ij} \tag{10}$$

In which G_{xy} is shear elastic modulus and θ is the rotation vector. Also, C_{ijkl} is the elastic constant, l is a material internal length scale parameter that is related to size effect. The length scale parameter showed effect of small size and could be taken values in between zero to unspecified positive micro/nano values which have to be determined in laboratory for various nanomaterials under many situations. The parameter for nanomaterials has not been already determined and by using a nondimensional form of this parameter it can be correctly used. In order to physically explain the length scale parameter, it is worth defining that the parameter depends on the crystal structure and the nature of physics of the material. As a physical interpretation, the domain of the applicability of classical field theories is intimately connected to the length and time scales. If L denotes the external characteristic length (e.g., crack length, wave length, a length over which applied loads are smooth) and l denotes the internal characteristic length (e.g., granular distance, lattice parameter, distance between atoms) then the region $L/l>1$, classical field theories predict sufficiently accurate results. On the other hand, when $L/l\sim1$, classical theories fail and the non-classical theories must be taken into account for long-range interatomic attractions [29].

To confirm the Maxwell equation, the distribution of external electric potential for the present nanoplate model is assumed as a combination of a cosine and linear variation [28, 30-31].

$$\overline{\Phi}(x,y,z) = -\cos(\beta z)\Phi(x,y) + \frac{2zV_0}{h} \tag{11}$$

where $\beta = \pi / h$ and $\Phi(x,y)$ is the spatial of the electric potential in the mid-plane of the nanoplate, and also V_0 is the external electric voltage. Then, the components of electric field can be written as:

$$E_k = \begin{Bmatrix} \overline{E}_x = -\dfrac{\partial \overline{\Phi}}{\partial x} \\ \overline{E}_y = -\dfrac{\partial \overline{\Phi}}{\partial y} \\ \overline{E}_z = -\dfrac{\partial \overline{\Phi}}{\partial z} \end{Bmatrix} = \begin{Bmatrix} \cos(\beta z)\dfrac{\partial \Phi}{\partial x} \\ \cos(\beta z)\dfrac{\partial \Phi}{\partial y} \\ -\beta \sin(\beta z)\Phi - \dfrac{2V_0}{h} \end{Bmatrix} \tag{12a-c}$$

$$\begin{Bmatrix} \overline{D}_x \\ \overline{D}_y \\ \overline{D}_z \end{Bmatrix} = \int_{-h/2}^{h/2} \begin{Bmatrix} D_x \cos(\beta z) \\ D_y \cos(\beta z) \\ D_z \beta \sin(\beta z) \end{Bmatrix} dz = \begin{Bmatrix} E_{15}\dfrac{\partial w_s}{\partial x} + X_{11}\dfrac{\partial \Phi}{\partial x} \\ E_{15}\dfrac{\partial w_s}{\partial y} + X_{11}\dfrac{\partial \Phi}{\partial y} \\ -E_{31}\dfrac{\partial^2 w_b}{\partial x^2} - E_{31}\dfrac{\partial^2 w_b}{\partial y^2} - X_{33}\Phi \end{Bmatrix} \tag{13a-c}$$

The coefficients in Eqs. (13) can be expressed respectively.

$$\begin{Bmatrix} E_{31} \\ E_{15} \\ X_{11} \\ X_{33} \end{Bmatrix} = \int_{-h/2}^{h/2} \begin{Bmatrix} \bar{e}_{31}\beta z \sin(\beta z) \\ \bar{e}_{15}\cos(\beta z) \\ \bar{\kappa}_{11}\cos^2(\beta z) \\ \bar{\kappa}_{33}\beta^2 \sin^2(\beta z) \end{Bmatrix} dz \tag{14a-d}$$

Here, to define a thermal stress function within which thermal stresses are a function of length and width of the plate, the following function is employed [32]:

$$F_0 = \frac{1}{48} Ly^2 \bar{\lambda}_{11} \Delta T \left(1 - \frac{12y^2}{Ly^2} + \frac{16y^3}{Ly^3}\right)\left(B_1 \times \sinh\left(R_1 \frac{2x}{Lx}\right) \times \sin\left(R_2 \frac{2x}{Lx}\right) + B_2 \times \cosh\left(R_1 \frac{2x}{Lx}\right) \times \cos\left(R_2 \frac{2x}{Lx}\right) + 1\right);$$

$$-\frac{Ly}{2} \le y \le 0 \tag{15}$$

(F_0: stress function defining thermal stresses in an unbuckled plate)

in which B_1, B_2, R_1 and R_2 are defined in the following:

$$B_1 = \frac{k_1 \times \sinh R_1 \times \cos R_2 - k_2 \times \cosh R_1 \times \sin R_2}{k_1 \times \sin R_2 \times \cos R_2 + k_2 \times \sinh R_1 \times \cosh R_2} \tag{16a}$$

$$B_2 = -\frac{k_1 \times \cosh R_1 \times \sin R_2 - k_2 \times \sinh R_1 \times \cos R_2}{k_1 \times \sin R_2 \times \cos R_2 + k_2 \times \sinh R_1 \times \cosh R_1} \tag{16b}$$

$$R_1 = k_1 \beta \tag{17a}$$

$$R_2 = k_2 \beta \tag{17b}$$

$$\beta = \frac{Lx}{Ly} \tag{18}$$

$$k_1 = \sqrt{\frac{4\left(21+\sqrt{1365}\right)}{13Ly^2}} \tag{19a}$$

$$k_2 = \sqrt{\frac{4\left(-21+\sqrt{1365}\right)}{13Ly^2}} \tag{19b}$$

The main reason for use of the above-mentioned stress function is the measurement of thermal stresses induced in a flat plate subjected to a ***known steady-state temperature gradient***. This temperature distribution was validated experimentally [32]. Note that the function is far from the real function of heat transfer in a nanomaterial related to its atomic structure. Although the function was used for a local continuum material (ALa), the function is an approximate mathematical relation which was made based on the following assumptions to show a known and a comprehensive heat transfer in a plate [33]:

1. Temperatures in the plate are constant through the thickness and distributed in a tent like manner over the faces (Fig. 2).
2. No external loads are applied and the plate is free to expand in all directions so that all stresses are due to the uniform temperature distribution.
3. The properties of the material do not vary with temperature and the stresses are within the elastic range.
4. Elastic displacements are small.
5. Shear stress due to temperature distribution is supposed to be appeared on the plate ($\sigma_{xy}^{T_0} \neq 0$).

To the best of the author's knowledge, in all of the thermal buckling studies in the literature, the thermal buckling relation resulted from the axial thermal strain (αΔT). For an instance, ref. [11] in which thermal buckling of double-layered orthotropic graphene nanoplates was studied. So, as it can be seen in Eq. (51) in the ref. [11], the thermal buckling functions are not related to the kind of material. This means that if the mechanical properties of e.g., steel alloys, aluminum alloys, etc. were used in Eq. (51), it can be employed for macro materials, and also if the mechanical properties of nanoplates were used, it can therefore be employed for nanomaterials. Of course, the function should be different between macro and nanomaterials, and for either of nanomaterials a function should be used which shows the heat transfer between the atoms of nanostructure in a real form (because either of nanomaterials has a specific atomic lattice with different interatomic behavior). But, there has never been presented such a function for a nanomaterial and a general function has to be employed. Similar formulations can be seen in other references in which thermal buckling has been studied.

The thermal stress in the plate which resulted from Eq. (15) is given by:

$$\sigma_x^{T_0} = \frac{\partial^2 F_0}{\partial y^2} = \bar{\lambda}_{11}\Delta T\left(\frac{2y}{Ly}-\frac{1}{2}\right)\left(B_1\times\sinh\left(R_1\frac{2x}{Lx}\right)\times\sin\left(R_2\frac{2x}{Lx}\right)+B_2\times\cosh\left(R_1\frac{2x}{Lx}\right)\times\cos\left(R_2\frac{2x}{Lx}\right)+1\right) \tag{20}$$

$$\sigma_y^{T_0} = \frac{\partial^2 F_0}{\partial x^2} = \frac{1}{12}\bar{\lambda}_{11}\Delta T\left(1-\frac{12y^2}{Ly^2}+\frac{16y^3}{Ly^3}\right)\left(D_1\times\sinh\left(R_1\frac{2x}{Lx}\right)\times\sin\left(R_2\frac{2x}{Lx}\right)+D_2\times\cosh\left(R_1\frac{2x}{Lx}\right)\times\cos\left(R_2\frac{2x}{Lx}\right)\right) \tag{21}$$

$$\sigma_{xy}^{T_0} = -\frac{\partial^2 F_0}{\partial x\,\partial y} = \frac{1}{2}\bar{\lambda}_{11}\Delta T\left(1-\frac{4y^2}{Ly^2}\right)\left(D_3\times\sinh\left(R_1\frac{2x}{Lx}\right)\times\cos\left(R_2\frac{2x}{Lx}\right)+D_4\times\cosh\left(R_1\frac{2x}{Lx}\right)\times\sin\left(R_2\frac{2x}{Lx}\right)\right) \tag{22}$$

$$-\frac{Ly}{2} \le y \le 0$$

where $\bar{\lambda}_{11}$ and ΔT are thermal modulus and temperature changes (For the current nanoplate at reference temperature T, the temperature rises uniformly to the final temperature T_0 which $\Delta T=T_0-T$ (T=300 K: Normal room temperature) [11]), Also, D_1, D_2, D_3 and D_4 are described as:

$$D_1 = B_1\left(k_1^2 - k_2^2\right) - 2B_2k_1k_2 \tag{23a}$$

$$D_2 = B_2\left(k_1^2 - k_2^2\right) + 2B_1k_1k_2 \tag{23b}$$

$$D_3 = B_1k_2 + B_2k_1 \tag{23c}$$

$$D_4 = B_1k_1 - B_2k_2 \tag{23d}$$

The temperature $\Delta\chi$ is distributed similar to a tent on the faces and $\Delta\zeta$ is the constant temperature along thickness of the plate (in the present study, it was assumed $\Delta\chi=\Delta\zeta=\Delta T$).

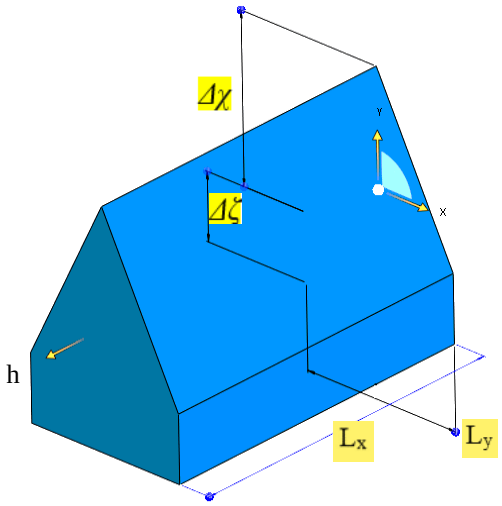

Fig. 2. Tent like temperature distribution according to the Eq. (15) [32-33]

Here, by integrating Eqs. (20-22) with respect to the x and y, the temperature differential over three dimensions of the plate are derived as [33]:

$$\delta U_{Complementary} = h\iint_A\left[\sigma_x^{T_0}\left(\frac{\partial^2 wi}{\partial x^2}\right)+\sigma_y^{T_0}\left(\frac{\partial^2 wi}{\partial x^2}\right)+\sigma_{xy}^{T_0}\left(\frac{\partial^2 wi}{\partial x\,\partial y}\right)\right]\delta wi\;\; dxdy\,,\;\; i=b,s \tag{24}$$

$$N_x^{T_0} = -\frac{\bar{\lambda}_{11}\Delta ThLx}{2}\left\{\left[B_1\frac{1}{(a)^2+(b)^2}\left(a\cos(c)\sin(d)-b\sinh(c)\cos(d)\right)+B_2\frac{1}{(a)^2+(b)^2}\left(a\sinh(c)\cos(d)+b\cosh(c)\sin(d)\right)\right]\right.$$
$$\left.-\left[B_1\frac{1}{(a)^2+(b)^2}\left(a\cosh(-c)\sin(-d)-b\sinh(-c)\cos(-d)\right)+B_2\frac{1}{(a)^2+(b)^2}\left(a\sinh(-c)\cos(-d)+b\cosh(-c)\sin(-d)\right)\right]\right\}$$

$$N_y^{T_0} = \frac{1}{12}\bar{\lambda}_{11}\Delta ThLx\left(1-\beta^2\right)\left\{\left[D_1\frac{1}{(a)^2+(b)^2}\left(a\cos(c)\sin(d)-b\sinh(c)\cos(d)\right)+D_2\frac{1}{(a)^2+(b)^2}\left(a\sinh(c)\cos(d)+b\cosh(c)\sin(d)\right)\right]\right.$$
$$\left.-\left[D_1\frac{1}{(a)^2+(b)^2}\left(a\cosh(-c)\sin(-d)-b\sinh(-c)\cos(-d)\right)+D_2\frac{1}{(a)^2+(b)^2}\left(a\sinh(-c)\cos(-d)+b\cosh(-c)\sin(-d)\right)\right]\right\}$$

$$N_{xy}^{T_0} = -\frac{7}{8}\bar{\lambda}_{11}\Delta T h L x\,\beta\left\{\left[D_3\frac{1}{(a)^2+(b)^2}\left(a\cosh(c)\cos(d)+b\sinh(c)\sin(d)\right)+D_4\frac{1}{(a)^2+(b)^2}\left(a\sinh(c)\sin(d)-b\cosh(c)\cos(d)\right)\right]\right.$$

$$\left.-\left[D_3\frac{1}{(a)^2+(b)^2}\left(a\cosh(-c)\cos(-d)+b\sinh(-c)\sin(-d)\right)+D_4\frac{1}{(a)^2+(b)^2}\left(a\sinh(-c)\sin(-d)-b\cosh(-c)\cos(-d)\right)\right]\right\}$$

(25a-c)

In which:

$$a=\frac{2k_1}{Ly};\ b=\frac{2k_2}{Ly};\ c=\frac{k_1}{2};\ d=\frac{k_2}{2} \tag{26}$$

Using the variational formulation the nonlinear constitutive equations are derived as follows:

$$\delta S = \iiint_v \begin{Bmatrix} \left(\sigma_{xx}^T+\sigma_{xx}^M\right)\delta\varepsilon_{xx} \\ \left(\sigma_{yy}^T+\sigma_{yy}^M\right)\delta\varepsilon_{yy} \\ \left(\tau_{xy}^T+\tau_{xy}^M\right)\delta\gamma_{xy} \\ \tau_{yz}\,\delta\gamma_{yz} \\ \tau_{xz}\,\delta\gamma_{xz} \end{Bmatrix} dV =$$

$$\iiint_v \begin{Bmatrix} \sigma_{xx}^T\delta\frac{\partial u}{\partial x}-\sigma_{xx}^T\delta\left(z\frac{\partial^2 w_b}{\partial x^2}\right)+\sigma_{xx}^T\delta\left[\frac{1}{2}\left(\frac{\partial w_b}{\partial x}\right)^2\right]+\sigma_{xx}^T\delta\left[\frac{1}{2}\left(\frac{\partial w_s}{\partial x}\right)^2\right]+\sigma_{xx}^T\delta\left(\frac{\partial w_b}{\partial x}\frac{\partial w_s}{\partial x}\right) \\ \sigma_{xx}^M\delta\frac{\partial u}{\partial x}-\sigma_{xx}^M\delta\left(z\frac{\partial^2 w_b}{\partial x^2}\right)+\sigma_{xx}^M\delta\left[\frac{1}{2}\left(\frac{\partial w_b}{\partial x}\right)^2\right]+\sigma_{xx}^M\delta\left[\frac{1}{2}\left(\frac{\partial w_s}{\partial x}\right)^2\right]+\sigma_{xx}^M\delta\left(\frac{\partial w_b}{\partial x}\frac{\partial w_s}{\partial x}\right) \\ \sigma_{yy}^T\delta\frac{\partial v}{\partial y}-\sigma_{yy}^T\delta\left(z\frac{\partial^2 w_b}{\partial y^2}\right)+\sigma_{yy}^T\delta\left[\frac{1}{2}\left(\frac{\partial w_b}{\partial y}\right)^2\right]+\sigma_{yy}^T\delta\left[\frac{1}{2}\left(\frac{\partial w_s}{\partial y}\right)^2\right]+\sigma_{yy}^T\delta\left(\frac{\partial w_b}{\partial y}\frac{\partial w_s}{\partial y}\right) \\ \sigma_{yy}^M\delta\frac{\partial v}{\partial y}-\sigma_{yy}^M\delta\left(z\frac{\partial^2 w_b}{\partial y^2}\right)+\sigma_{yy}^M\delta\left[\frac{1}{2}\left(\frac{\partial w_b}{\partial y}\right)^2\right]+\sigma_{yy}^M\delta\left[\frac{1}{2}\left(\frac{\partial w_s}{\partial y}\right)^2\right]+\sigma_{yy}^M\delta\left(\frac{\partial w_b}{\partial y}\frac{\partial w_s}{\partial y}\right) \\ \tau_{xy}^T\delta\left(\frac{\partial u}{\partial y}+\frac{\partial v}{\partial x}\right)-\tau_{xy}^T\delta\left(2z\frac{\partial^2 w_b}{\partial x\,\partial y}\right)+\tau_{xy}^T\delta\left[\left(\frac{\partial w_b}{\partial x}+\frac{\partial w_s}{\partial x}\right)\left(\frac{\partial w_b}{\partial y}+\frac{\partial w_s}{\partial y}\right)\right] \\ \tau_{xy}^M\delta\left(\frac{\partial u}{\partial y}+\frac{\partial v}{\partial x}\right)-\tau_{xy}^M\delta\left(2z\frac{\partial^2 w_b}{\partial x\,\partial y}\right)+\tau_{xy}^M\delta\left[\left(\frac{\partial w_b}{\partial x}+\frac{\partial w_s}{\partial x}\right)\left(\frac{\partial w_b}{\partial y}+\frac{\partial w_s}{\partial y}\right)\right] \\ \tau_{yz}\,\delta\frac{\partial w_s}{\partial y} \\ \tau_{xz}\,\delta\frac{\partial w_s}{\partial x} \end{Bmatrix} dV = 0 \tag{27}$$

$$\delta S_1 = \iiint_v \begin{Bmatrix} \sigma_{xx}^T\frac{\partial}{\partial x}\delta u - z\,\sigma_{xx}^T\frac{\partial^2}{\partial x^2}\delta w_b+\sigma_{xx}^T\frac{\partial w_b}{\partial x}\frac{\partial}{\partial x}\delta w_b+\sigma_{xx}^T\frac{\partial w_s}{\partial x}\frac{\partial}{\partial x}\delta w_s+\sigma_{xx}^T\left(\frac{\partial w_s}{\partial x}\frac{\partial}{\partial x}\delta w_b+\frac{\partial w_b}{\partial x}\frac{\partial}{\partial x}\delta w_s\right) \\ \sigma_{yy}^T\frac{\partial}{\partial y}\delta v - z\,\sigma_{yy}^T\frac{\partial^2}{\partial y^2}\delta w_b+\sigma_{yy}^T\frac{\partial w_b}{\partial y}\frac{\partial}{\partial y}\delta w_b+\sigma_{yy}^T\frac{\partial w_s}{\partial y}\frac{\partial}{\partial y}\delta w_s+\sigma_{yy}^T\left(\frac{\partial w_s}{\partial y}\frac{\partial}{\partial y}\delta w_b+\frac{\partial w_b}{\partial y}\frac{\partial}{\partial y}\delta w_s\right) \end{Bmatrix} dV = 0$$

(28)

$$\delta S_2 = \iiint_v \left[\tau_{xy}^T \left(\frac{\partial}{\partial y}\delta u + \frac{\partial}{\partial x}\delta v \right) - 2\tau_{xy}^T z \left(\frac{\partial^2}{\partial x\,\partial y}\delta w_b \right) + \tau_{xy}^T \left(\frac{\partial w_b}{\partial x}\frac{\partial}{\partial y}\delta w_b + \frac{\partial w_b}{\partial y}\frac{\partial}{\partial x}\delta w_b \right) + \tau_{xy}^T \left(\frac{\partial w_s}{\partial y}\frac{\partial}{\partial x}\delta w_b + \frac{\partial w_b}{\partial x}\frac{\partial}{\partial y}\delta w_s \right) \right.$$
$$\left. + \tau_{xy}^T \left(\frac{\partial w_s}{\partial x}\frac{\partial}{\partial y}\delta w_b + \frac{\partial w_b}{\partial y}\frac{\partial}{\partial x}\delta w_s \right) + \tau_{xy}^T \left(\frac{\partial w_s}{\partial x}\frac{\partial}{\partial y}\delta w_s + \frac{\partial w_s}{\partial y}\frac{\partial}{\partial x}\delta w_s \right) \right] = 0 \tag{29}$$

The work of external forces is expressed as follows (Index 1 is used for the upper layer and index 2 for the lower layer, respectively) [34]:

$$\delta\Omega_i = \int_0^{L_y}\int_0^{L_x} k_o\left(\left(w_b j + w_s j\right) - \left(w_b i + w_s i\right)\right)\delta w_i dx dy \;;\; i=1,\, j=2 \tag{30}$$

$$\delta\Omega_j = \int_0^{L_y}\int_0^{L_x} \left(-k_o\left(\left(w_b j + w_s j\right) - \left(w_b i + w_s i\right)\right) - k_w\left(w_b j + w_s j\right) + k_G\nabla^2\left(w_b j + w_s j\right)\right)\delta w_j dx dy \;;\; i=1,\, j=2 \tag{31}$$

where k_w and k_G denote the Winkler and Pasternak stiffness coefficients of the elastic matrix, and k_o represents the van der Waals (vdW) interaction bonds between the layers. Finally, the thermal stability equations will be derived using the principle of minimum total potential energy (δV=0) in the following equations:

$$\begin{bmatrix} \delta w_s \\ \delta w_b \\ \delta\Phi \end{bmatrix} = 0 :$$

$$\begin{bmatrix}
\frac{\partial Q_x}{\partial x} + \frac{\partial Q_y}{\partial y} - N_{xx}^T\left(\frac{\partial^2 w_s}{\partial x^2} + \frac{\partial^2 w_b}{\partial x^2}\right) - N_{yy}^T\left(\frac{\partial^2 w_s}{\partial y^2} + \frac{\partial^2 w_b}{\partial y^2}\right) + 2N_{xy}^T\left(\frac{\partial^2 w_s}{\partial x\,\partial y} + \frac{\partial^2 w_b}{\partial x\,\partial y}\right) - \frac{1}{2}\frac{\partial^2 Y_{xx}}{\partial x\,\partial y} + \frac{1}{2}\frac{\partial^2 Y_{yy}}{\partial x\,\partial y} - \frac{1}{4}\frac{\partial^2 Y_{xy}}{\partial y^2} + \frac{1}{4}\frac{\partial^2 Y_{xy}}{\partial x^2} = 0 \\
-\frac{\partial^2 M_x}{\partial x^2} - 2\frac{\partial^2 M_{xy}}{\partial x\,\partial y} - \frac{\partial^2 M_y}{\partial y^2} - \frac{\partial^2 M_x^T}{\partial x^2} - 2\frac{\partial^2 M_{xy}^T}{\partial x\,\partial y} - \frac{\partial^2 M_y^T}{\partial y^2} - N_{xx}^T\left(\frac{\partial^2 w_s}{\partial x^2} + \frac{\partial^2 w_b}{\partial x^2}\right) - N_{yy}^T\left(\frac{\partial^2 w_s}{\partial y^2} + \frac{\partial^2 w_b}{\partial y^2}\right) + 2N_{xy}^T\left(\frac{\partial^2 w_s}{\partial x\,\partial y} + \frac{\partial^2 w_b}{\partial x\,\partial y}\right) \\
-\frac{\partial^2 Y_{xx}}{\partial x\,\partial y} + \frac{\partial^2 Y_{yy}}{\partial x\,\partial y} - \frac{1}{2}\frac{\partial^2 Y_{xy}}{\partial y^2} + \frac{1}{2}\frac{\partial^2 Y_{xy}}{\partial x^2} = 0 \\
\int_{-h/2}^{h/2}\left[\frac{\partial \overline{D}_x}{\partial x}\cos(\beta z) + \frac{\partial \overline{D}_y}{\partial y}\cos(\beta z) + \overline{D}_z\,\beta\sin(\beta z)\right]dz = 0
\end{bmatrix} \tag{32a-c}$$

N_i, M_i, and Q_i *(i= x, y, xy)* are axial, moment and shear stress resultants, respectively, and also Y_{ij} *(i= x, y, xy)* are non-zero curvature resultants.

On the other hand, the non-classical boundary conditions originated from the couple stress theory are obtained as:

$$\int_0^{Lx}\left\{\left(\frac{1}{2}\frac{\partial Y_{xx}}{\partial x} + \frac{1}{4}\frac{\partial Y_{xy}}{\partial y}\right)\delta w_s + \left(\frac{\partial Y_{xx}}{\partial x} + \frac{1}{2}\frac{\partial Y_{xy}}{\partial y}\right)\delta w_b\right\}dx = 0 \tag{33a}$$

$$\int_0^{Ly} -\left\{\left(\frac{1}{2}\frac{\partial Y_{yy}}{\partial y} + \frac{1}{4}\frac{\partial Y_{xy}}{\partial x}\right)\delta w_s + \left(\frac{\partial Y_{yy}}{\partial y} + \frac{1}{2}\frac{\partial Y_{xy}}{\partial x}\right)\delta w_b\right\}dy = 0 \tag{33b}$$

In Eqs. (32) the bending moments raised from temperature are as follows:

$$(M_x^T, M_y^T, M_{xy}^T) = \lambda_{11}\int_{-h/2}^{h/2}\Delta T(i,j,k)\,z dz = 0 \;;\; \text{uniform temperature distribution} \tag{34a}$$

$$(M_x^T, M_y^T, M_{xy}^T) = \lambda_{11}\int_{-h/2}^{h/2}\Delta T(i,j,k)\,z dz \neq 0 \;;\; \text{nonuniform temperature distribution} \tag{34b}$$

Thereafter, the stress resultants and non-zero curvature resultants are expressed as:

$$\begin{Bmatrix} N_x \\ N_y \\ N_{xy} \\ M_x \\ M_y \\ M_{xy} \\ Q_x \\ Q_y \end{Bmatrix} = \int_{-h/2}^{h/2} \begin{Bmatrix} \sigma_x \\ \sigma_y \\ \sigma_{xy} \\ z\sigma_x \\ z\sigma_y \\ z\sigma_{xy} \\ \sigma_{xz} \\ \sigma_{yz} \end{Bmatrix} dz = \begin{bmatrix} A_{11} & A_{12} & 0 & 0 & 0 & 0 & 0 & 0 \\ A_{21} & A_{22} & 0 & 0 & 0 & 0 & 0 & 0 \\ 0 & 0 & A_{66} & 0 & 0 & 0 & 0 & 0 \\ 0 & 0 & 0 & D_{11} & D_{12} & 0 & 0 & 0 \\ 0 & 0 & 0 & D_{21} & D_{22} & 0 & 0 & 0 \\ 0 & 0 & 0 & 0 & 0 & D_{66} & 0 & 0 \\ 0 & 0 & 0 & 0 & 0 & 0 & A_{44} & 0 \\ 0 & 0 & 0 & 0 & 0 & 0 & 0 & A_{44} \end{bmatrix} \times \begin{bmatrix} \frac{\partial u}{\partial x} + \frac{1}{2}\left(\frac{\partial w_b}{\partial x}\right)^2 + \frac{1}{2}\left(\frac{\partial w_s}{\partial x}\right)^2 + \frac{\partial w_b}{\partial x}\frac{\partial w_s}{\partial x} \\ \frac{\partial v}{\partial y} + \frac{1}{2}\left(\frac{\partial w_b}{\partial y}\right)^2 + \frac{1}{2}\left(\frac{\partial w_s}{\partial y}\right)^2 + \frac{\partial w_b}{\partial y}\frac{\partial w_s}{\partial y} \\ \frac{\partial u}{\partial y} + \frac{\partial v}{\partial x} + \left(\frac{\partial w_b}{\partial x} + \frac{\partial w_s}{\partial x}\right)\left(\frac{\partial w_b}{\partial y} + \frac{\partial w_s}{\partial y}\right) \\ -\frac{\partial^2 w_b}{\partial x^2} \\ -\frac{\partial^2 w_b}{\partial y^2} \\ -\frac{\partial^2 w_b}{\partial x \partial y} \\ \frac{\partial w_s}{\partial x} \\ \frac{\partial w_s}{\partial y} \end{bmatrix} \tag{35a-h}$$

$$\begin{Bmatrix} Y_{xx} \\ Y_{yy} \\ Y_{xy} \\ Y_{xz} \\ Y_{yz} \end{Bmatrix} = \int_{-h/2}^{h/2} \begin{Bmatrix} m_{xx} \\ m_{yy} \\ m_{xy} \\ m_{xz} \\ m_{yz} \end{Bmatrix} dz = l^2 h \bar{C}_{66} \times \begin{Bmatrix} \left(2\frac{\partial^2 w_b}{\partial x \partial y} + \frac{\partial^2 w_s}{\partial x \partial y}\right) \\ \left(-2\frac{\partial^2 w_b}{\partial x \partial y} - \frac{\partial^2 w_s}{\partial x \partial y}\right) \\ \frac{1}{2}\left(-2\frac{\partial^2 w_b}{\partial x^2} + 2\frac{\partial^2 w_b}{\partial y^2} - \frac{\partial^2 w_s}{\partial x^2} + \frac{\partial^2 w_s}{\partial y^2}\right) \\ \frac{1}{2}\left(\frac{\partial^2 v}{\partial x^2} - \frac{\partial^2 u}{\partial x \partial y}\right) \\ \frac{1}{2}\left(-\frac{\partial^2 u}{\partial y^2} + \frac{\partial^2 v}{\partial x \partial y}\right) \end{Bmatrix} \tag{36a-e}$$

The in-plane stress resultants are explained as follows:

$$\left[N_{ij}\right]^{Total} = \left[N_{ij}\right]^{Mech.} + \left[N_{ij}\right]^{Elec.} + \left[N_{ij}\right]^{T_0} \tag{37}$$

where N_x^E and N_y^E are the in-plane electric loads as [35-36]:

$$N_x^E, N_y^E = \int_{-h/2}^{h/2} \bar{e}_{31} \frac{2V_0}{h} dz \tag{38}$$

Also $\left[N_{ij}\right]^{Mech.}$ are neglected in the present research and $\left[N_{ij}\right]^{T_0}$ are mentioned in Eqs. 25. The stress resultants in displacement field by using Eqs. (35) and (37) are redefined in the following:

$$\begin{bmatrix} N_{xx} \\ N_{yy} \\ N_{xy} \\ M_{xx} \\ M_{yy} \\ M_{xy} \\ Q_x \\ Q_y \end{bmatrix} = \begin{bmatrix} A_{11} & A_{12} & 0 & 0 & 0 & 0 & 0 & 0 \\ A_{21} & A_{22} & 0 & 0 & 0 & 0 & 0 & 0 \\ 0 & 0 & A_{66} & 0 & 0 & 0 & 0 & 0 \\ 0 & 0 & 0 & D_{11} & D_{12} & 0 & 0 & 0 \\ 0 & 0 & 0 & D_{21} & D_{22} & 0 & 0 & 0 \\ 0 & 0 & 0 & 0 & 0 & D_{66} & 0 & 0 \\ 0 & 0 & 0 & 0 & 0 & 0 & A_{44} & 0 \\ 0 & 0 & 0 & 0 & 0 & 0 & 0 & A_{44} \end{bmatrix} \times \begin{bmatrix} \frac{\partial u}{\partial x} + \frac{1}{2}\left(\frac{\partial w_b}{\partial x}\right)^2 + \frac{1}{2}\left(\frac{\partial w_s}{\partial x}\right)^2 + \frac{\partial w_b}{\partial x}\frac{\partial w_s}{\partial x} \\ \frac{\partial v}{\partial y} + \frac{1}{2}\left(\frac{\partial w_b}{\partial y}\right)^2 + \frac{1}{2}\left(\frac{\partial w_s}{\partial y}\right)^2 + \frac{\partial w_b}{\partial y}\frac{\partial w_s}{\partial y} \\ \frac{\partial u}{\partial y} + \frac{\partial v}{\partial x} + \left(\frac{\partial w_b}{\partial x} + \frac{\partial w_s}{\partial x}\right)\left(\frac{\partial w_b}{\partial y} + \frac{\partial w_s}{\partial y}\right) \\ -\frac{\partial^2 w_b}{\partial x^2} \\ -\frac{\partial^2 w_b}{\partial y^2} \\ -\frac{\partial^2 w_b}{\partial x \partial y} \\ \frac{\partial w_s}{\partial x} \\ \frac{\partial w_s}{\partial y} \end{bmatrix} + \begin{Bmatrix} 2\bar{e}_{31}V_0 \\ 2\bar{e}_{31}V_0 \\ 0 \\ E_{31}\Phi \\ E_{31}\Phi \\ 0 \\ -E_{15}\frac{\partial \Phi}{\partial x} \\ -E_{15}\frac{\partial \Phi}{\partial y} \end{Bmatrix} - \begin{Bmatrix} N_x^{T_0} \\ N_y^{T_0} \\ N_{xy}^{T_0} \\ 0 \\ 0 \\ 0 \\ 0 \\ 0 \end{Bmatrix} \quad \text{(39a-h)}$$

In Eqs. (39), A_{ij} and D_{ij} are extensional stiffness and extension-bending coupling matrix respectively, as follows:

$$A_{ij} = \int_{-\frac{h}{2}}^{\frac{h}{2}} \bar{C}_{ij}\, dz \quad (i,j = 1,2,4,6)\ ,\ D_{ij} = \int_{-\frac{h}{2}}^{\frac{h}{2}} \bar{C}_{ij} z^2\, dz \quad (i,j = 1,2,6) \quad \text{(40a-b)}$$

$$\begin{Bmatrix} \bar{C}_{11} \\ \bar{C}_{12} \\ \bar{C}_{44} \\ \bar{C}_{66} \end{Bmatrix} = \begin{Bmatrix} C_{11} - \frac{C_{13}^2}{C_{33}} \\ C_{12} - \frac{C_{13}^2}{C_{33}} \\ C_{44} \\ C_{66} \end{Bmatrix} \quad \text{(41a-d)}$$

$$\begin{Bmatrix} \bar{e}_{31} \\ \bar{e}_{15} \\ \bar{\kappa}_{11} \\ \bar{\kappa}_{33} \end{Bmatrix} = \begin{Bmatrix} e_{31} - \frac{C_{13}e_{33}}{C_{33}} \\ e_{15} \\ \kappa_{11} \\ \kappa_{33} + \frac{e_{33}^2}{C_{33}} \end{Bmatrix} \quad \text{(42a-d)}$$

Inserting Eqs. (36, 39) into Eqs. (32), the thermal stability equations in the form of displacement components and based on S-FSDT also including couple stress effects for DLPNs are expressed which lead to Eqs. (43):

$$A_{44}\left(\frac{\partial^2 w_s i}{\partial x^2} + \frac{\partial^2 w_s i}{\partial y^2}\right) + \left(2\bar{e}_{31}V_0 - N_x^{T_0}\right) \times \left(\frac{\partial^2 w_b i}{\partial x^2} + \frac{\partial^2 w_s i}{\partial x^2}\right) + \left(2\bar{e}_{31}V_0 - N_y^{T_0}\right) \times \left(\frac{\partial^2 w_b i}{\partial y^2} + \frac{\partial^2 w_s i}{\partial y^2}\right) + 2N_{xy}^{T_0}\left(\frac{\partial^2 w_b i}{\partial x \partial y} + \frac{\partial^2 w_s i}{\partial x \partial y}\right) +$$

$$k_o\left(\left(w_b j + w_s j\right) - \left(w_b i + w_s i\right)\right) - E_{15}\frac{\partial^2 \Phi i}{\partial x^2} - E_{15}\frac{\partial^2 \Phi i}{\partial y^2} - A_s\left[\frac{3}{2}\left(\frac{\partial^4 w_b i}{\partial x^2 \partial y^2} + \frac{1}{2}\frac{\partial^4 w_s i}{\partial x^2 \partial y^2}\right) + \frac{1}{4}\left(\frac{\partial^4 w_b i}{\partial x^4} + \frac{1}{2}\frac{\partial^4 w_s i}{\partial x^4} + \frac{\partial^4 w_b i}{\partial y^4} + \frac{1}{2}\frac{\partial^4 w_s i}{\partial y^4}\right)\right] = 0$$

i=1, j=2

$$D_{11}\frac{\partial^4 w_b i}{\partial x^4}+D_{22}\frac{\partial^4 w_b i}{\partial y^4}+(2D_{12}+2D_{66})\frac{\partial^4 w_b i}{\partial x^2\partial y^2}+\left(2\bar{e}_{31}V_0-N_x^{T_0}\right)\times\left(\frac{\partial^2 w_b i}{\partial x^2}+\frac{\partial^2 w_s i}{\partial x^2}\right)+\left(2\bar{e}_{31}V_0-N_y^{T_0}\right)\times\left(\frac{\partial^2 w_b i}{\partial y^2}+\frac{\partial^2 w_s i}{\partial y^2}\right)+$$
$$k_o\left((w_b j+w_s j)-(w_b i+w_s i)\right)+2N_{xy}^{T_0}\left(\frac{\partial^2 w_b i}{\partial x\partial y}+\frac{\partial^2 w_s i}{\partial x\partial y}\right)+E_{31}\frac{\partial^2\Phi i}{\partial x^2}+E_{31}\frac{\partial^2\Phi i}{\partial y^2}-A_s\left[3\left(\frac{\partial^4 w_b i}{\partial x^2\partial y^2}+\frac{1}{2}\frac{\partial^4 w_s i}{\partial x^2\partial y^2}\right)+\right.$$
$$\left.\frac{1}{4}\left(2\frac{\partial^4 w_b i}{\partial x^4}+\frac{\partial^4 w_s i}{\partial x^4}+2\frac{\partial^4 w_b i}{\partial y^4}+\frac{\partial^4 w_s i}{\partial y^4}\right)\right]=0\ ;\ i=1, j=2$$

$$A_{44}\left(\frac{\partial^2 w_s j}{\partial x^2}+\frac{\partial^2 w_s j}{\partial y^2}\right)+\left(2\bar{e}_{31}V_0-N_x^{T_0}\right)\times\left(\frac{\partial^2 w_b j}{\partial x^2}+\frac{\partial^2 w_s j}{\partial x^2}\right)+\left(2\bar{e}_{31}V_0-N_y^{T_0}\right)\times\left(\frac{\partial^2 w_b j}{\partial y^2}+\frac{\partial^2 w_s j}{\partial y^2}\right)+2N_{xy}^{T_0}\left(\frac{\partial^2 w_b j}{\partial x\partial y}+\frac{\partial^2 w_s j}{\partial x\partial y}\right)$$
$$-k_o\left((w_b j+w_s j)-(w_b i+w_s i)\right)-k_w\left(w_b j+w_s j\right)+k_G\nabla^2\left(w_b j+w_s j\right)-E_{15}\frac{\partial^2\Phi j}{\partial x^2}-E_{15}\frac{\partial^2\Phi j}{\partial y^2}-A_s\left[\frac{3}{2}\left(\frac{\partial^4 w_b j}{\partial x^2\partial y^2}+\frac{1}{2}\frac{\partial^4 w_s j}{\partial x^2\partial y^2}\right)\right.$$
$$\left.+\frac{1}{4}\left(\frac{\partial^4 w_b j}{\partial x^4}+\frac{1}{2}\frac{\partial^4 w_s j}{\partial x^4}+\frac{\partial^4 w_b j}{\partial y^4}+\frac{1}{2}\frac{\partial^4 w_s j}{\partial y^4}\right)\right]=0\ ;\ \ i=1, j=2$$

$$D_{11}\frac{\partial^4 w_b j}{\partial x^4}+D_{22}\frac{\partial^4 w_b j}{\partial y^4}+(2D_{12}+2D_{66})\frac{\partial^4 w_b j}{\partial x^2\partial y^2}+\left(2\bar{e}_{31}V_0-N_x^{T_0}\right)\times\left(\frac{\partial^2 w_b j}{\partial x^2}+\frac{\partial^2 w_s j}{\partial x^2}\right)+\left(2\bar{e}_{31}V_0-N_y^{T_0}\right)\times\left(\frac{\partial^2 w_b j}{\partial y^2}+\frac{\partial^2 w_s j}{\partial y^2}\right)-$$
$$k_o\left((w_b j+w_s j)-(w_b i+w_s i)\right)-k_w\left(w_b j+w_s j\right)+k_G\nabla^2\left(w_b j+w_s j\right)+2N_{xy}^{T_0}\left(\frac{\partial^2 w_b j}{\partial x\partial y}+\frac{\partial^2 w_s j}{\partial x\partial y}\right)+E_{31}\frac{\partial^2\Phi j}{\partial x^2}+E_{31}\frac{\partial^2\Phi j}{\partial y^2}-$$
$$A_s\left[3\left(\frac{\partial^4 w_b j}{\partial x^2\partial y^2}+\frac{1}{2}\frac{\partial^4 w_s j}{\partial x^2\partial y^2}\right)+\frac{1}{4}\left(2\frac{\partial^4 w_b j}{\partial x^4}+\frac{\partial^4 w_s j}{\partial x^4}+2\frac{\partial^4 w_b j}{\partial y^4}+\frac{\partial^4 w_s j}{\partial y^4}\right)\right]=0\ ;\ i=1, j=2$$

$$E_{15}\left(\frac{\partial^2 w_s i}{\partial x^2}+\frac{\partial^2 w_s i}{\partial y^2}\right)-E_{31}\left(\frac{\partial^2 w_b i}{\partial x^2}+\frac{\partial^2 w_b i}{\partial y^2}\right)+X_{11}\left(\frac{\partial^2\Phi i}{\partial x^2}+\frac{\partial^2\Phi i}{\partial y^2}\right)-X_{33}\Phi i=0\ ;\ i=1,2$$

(43a-f)

In which A_s is defined by:

$$A_s=\int_{-\frac{h}{2}}^{\frac{h}{2}} l^2\bar{C}_{66}\ dz \tag{44}$$

3. Analytical solution

In this section, to obtain critical temperature of DLPNs with simply-supported and clamped boundary conditions (B.Cs) the essential and natural B.Cs are presented in the following [14, 37]:

Simply-supported (S):

$\Phi = w_b = w_s = M_x = 0;$ *at* $x = 0, L_x$ (45a)

$\Phi = w_b = w_s = M_y = 0;$ *at* $y = 0, L_y$ (45b)

Clamped (C):

$\Phi = w_b = w_s = 0;$ *at* $x = 0, L_x$ *and* $y = 0, L_y$ (46)

In order to solve the stability equations the Galerkin variational method has been used. In the method, the responses are assumed to be as follows:

$$w_s i\,(x,y)=\sum_{m=1}^{\infty}\sum_{n=1}^{\infty}A_{mn}i\,.\,X_{m,n}\ (x,y),\ i=1,2 \tag{47a}$$

$$w_b i\,(x,y)=\sum_{m=1}^{\infty}\sum_{n=1}^{\infty}B_{mn}i\,.\,X_{m,n}\ (x,y),\ i=1,2 \tag{47b}$$

$$\Phi i\,(x,y)=\sum_{m=1}^{\infty}\sum_{n=1}^{\infty}C_{mn}i\,.\,X_{m,n}\,(x,y),\ i=1,2 \tag{47c}$$

In which $X_{m,n}\,(x,y)$ are shape functions on the basis of *x* and *y* which satisfy the boundary conditions in Eqs. (45) and (46). And A_{mn}, B_{mn} and C_{mn} are the constant coefficients which should be calculated. The admissible shape functions are listed in Table. 1.

Table 1. Shape functions

Boundary conditions	$X_m\,(x)$	$Y_n\,(y)$
SSSS	$\mathrm{Sin}(\alpha x)$	$\mathrm{Sin}(\beta y)$
CCCC	$\mathrm{Sin}^2(\alpha x)$	$\mathrm{Sin}^2(\beta y)$

where $\alpha = m\pi/Lx$ and $\beta = n\pi/Ly$, *m* and *n* are the half-waves numbers. Substituting Eqs. (47) into Eqs. (43), a residual in the algebraic form will be obtained, based on the Galerkin approach, the residual must be perpendicular on the shape functions, which will be presented by:

$$\iint R\,(x,y)\,.\,X_{m,n}\,(x,y)\,dxdy=0,\ m,n=1,2,3,... \tag{48}$$

On the basis of Eq. (48), the homogenous algebraic equations system will be obtained as:

$$\begin{bmatrix} K_{11} & K_{12} & K_{13} & K_{14} & K_{15} & K_{16} \\ K_{21} & K_{22} & K_{23} & K_{24} & K_{25} & K_{26} \\ K_{31} & K_{32} & K_{33} & K_{34} & K_{35} & K_{36} \\ K_{41} & K_{42} & K_{43} & K_{44} & K_{45} & K_{46} \\ K_{51} & K_{52} & K_{53} & K_{54} & K_{55} & K_{56} \\ K_{61} & K_{62} & K_{63} & K_{64} & K_{65} & K_{66} \end{bmatrix} \begin{Bmatrix} A_1 \\ B_1 \\ C_1 \\ A_2 \\ B_2 \\ C_2 \end{Bmatrix} = 0 \tag{49}$$

where $(A_1, B_1, C_1, A_2, B_2, C_2)$ are the unknown variables. Also $\left[K_{ij}\right]$ are coefficients of unknown variables as follows:

$$K_{11}=\int_0^{Lx}\int_0^{Ly}\left[A_{44}\left(\frac{\partial^2 X_m}{\partial x^2}X_n+\frac{\partial^2 X_n}{\partial y^2}X_m\right)+\left(2\bar{e}_{31}V_0-N_x^{T_0}\right)\frac{\partial^2 X_m}{\partial x^2}X_n+\left(2\bar{e}_{31}V_0-N_y^{T_0}\right)\frac{\partial^2 X_n}{\partial y^2}X_m+2N_{xy}^{T_0}\frac{\partial^2 X_{m,n}}{\partial x\,\partial y}-k_o X_m X_n-\right.$$
$$\left.A_s\left(\frac{3}{4}\frac{\partial^4 X_{m,n}}{\partial x^2\partial y^2}+\frac{1}{8}\frac{\partial^4 X_m}{\partial x^4}X_n+\frac{1}{8}\frac{\partial^4 X_n}{\partial y^4}X_m\right)\right]X_m X_n dydx$$

$$K_{12}=\int_0^{Lx}\int_0^{Ly}\left[\left(2\bar{e}_{31}V_0-N_x^{T_0}\right)\left(\frac{\partial^2 X_m}{\partial x^2}X_n\right)+\left(2\bar{e}_{31}V_0-N_y^{T_0}\right)\left(\frac{\partial^2 X_n}{\partial y^2}X_m\right)+2N_{xy}^{T_0}\left(\frac{\partial^2 X_{m,n}}{\partial x\,\partial y}\right)-k_o X_m X_n-\right.$$
$$\left.A_s\left(\frac{3}{2}\frac{\partial^4 X_{m,n}}{\partial x^2\partial y^2}+\frac{1}{4}\frac{\partial^4 X_m}{\partial x^4}X_n+\frac{1}{4}\frac{\partial^4 X_n}{\partial y^4}X_m\right)\right]X_m X_n dydx$$

$$K_{13}=-E_{15}\int_0^{Lx}\int_0^{Ly}\left[\frac{\partial^2 X_m}{\partial x^2}X_n+\frac{\partial^2 X_n}{\partial y^2}X_m\right]X_m X_n dydx$$

$$K_{14}=k_o\int_0^{Lx}\int_0^{Ly}X_m^2 X_n^2 dydx$$

$$K_{15}=k_o\int_0^{Lx}\int_0^{Ly}X_m^2 X_n^2 dydx$$

$$K_{16}=0$$

$$K_{21}=\int_0^{Lx}\int_0^{Ly}\left[\left(2\bar{e}_{31}V_0-N_x^{T_0}\right)\frac{\partial^2 X_m}{\partial x^2}X_n+\left(2\bar{e}_{31}V_0-N_y^{T_0}\right)\frac{\partial^2 X_n}{\partial y^2}X_m-k_oX_mX_n+2N_{xy}^{T_0}\frac{\partial^2 X_{m,n}}{\partial x\,\partial y}-\right.$$
$$\left.A_s\left(\frac{3}{2}\frac{\partial^4 X_{m,n}}{\partial x^2\partial y^2}+\frac{1}{4}\frac{\partial^4 X_m}{\partial x^4}X_n+\frac{1}{4}\frac{\partial^4 X_n}{\partial y^4}X_m\right)\right]X_mX_n dydx$$

$$K_{22}=\int_0^{Lx}\int_0^{Ly}\left[D_{11}\frac{\partial^4 X_m}{\partial x^4}X_n+D_{22}\frac{\partial^4 X_n}{\partial y^4}X_m+\left(2D_{12}+2D_{66}\right)\frac{\partial^4 X_{m,n}}{\partial x^2\partial y^2}+\left(2\bar{e}_{31}V_0-N_x^{T_0}\right)\frac{\partial^2 X_m}{\partial x^2}X_n+\left(2\bar{e}_{31}V_0-N_y^{T_0}\right)\frac{\partial^2 X_n}{\partial y^2}X_m+\right.$$
$$\left.k_oX_mX_n+2N_{xy}^{T_0}\frac{\partial^2 X_{m,n}}{\partial x\,\partial y}-A_s\left(3\frac{\partial^4 X_{m,n}}{\partial x^2\partial y^2}+\frac{1}{2}\frac{\partial^4 X_m}{\partial x^4}X_n+\frac{1}{2}\frac{\partial^4 X_n}{\partial y^4}X_m\right)\right]X_mX_n dydx$$

$$K_{23}=E_{31}\int_0^{Lx}\int_0^{Ly}\left[\frac{\partial^2 X_m}{\partial x^2}X_n+\frac{\partial^2 X_n}{\partial y^2}X_m\right]X_mX_n dydx$$

$$K_{24}=k_o\int_0^{Lx}\int_0^{Ly}X_m^{\,2}X_n^{\,2}dydx$$

$$K_{25}=k_o\int_0^{Lx}\int_0^{Ly}X_m^{\,2}X_n^{\,2}dydx$$

$$K_{26}=0$$

$$K_{31}=E_{15}\int_0^{Lx}\int_0^{Ly}\left[\frac{\partial^2 X_m}{\partial x^2}X_n+\frac{\partial^2 X_n}{\partial y^2}X_m\right]X_mX_n dydx$$

$$K_{32}=-E_{31}\int_0^{Lx}\int_0^{Ly}\left[\frac{\partial^2 X_m}{\partial x^2}X_n+\frac{\partial^2 X_n}{\partial y^2}X_m\right]X_mX_n dydx$$

$$K_{33}=\int_0^{Lx}\int_0^{Ly}\left[X_{11}\left(\frac{\partial^2 X_m}{\partial x^2}X_n+\frac{\partial^2 X_n}{\partial y^2}X_m\right)-X_{33}X_mX_n\right]X_mX_n dydx$$

$$K_{34}=K_{35}=K_{36}=0$$

$$K_{41}=k_o\int_0^{Lx}\int_0^{Ly}X_m^{\,2}X_n^{\,2}dydx$$

$$K_{42}=k_o\int_0^{Lx}\int_0^{Ly}X_m^{\,2}X_n^{\,2}dydx$$

$$K_{43}=0$$

$$K_{44}=\int_0^{Lx}\int_0^{Ly}\left[A_{44}\left(\frac{\partial^2 X_m}{\partial x^2}X_n+\frac{\partial^2 X_n}{\partial y^2}X_m\right)+\left(2\bar{e}_{31}V_0-N_x^{T_0}\right)\frac{\partial^2 X_m}{\partial x^2}X_n+\left(2\bar{e}_{31}V_0-N_y^{T_0}\right)\frac{\partial^2 X_n}{\partial y^2}X_m+2N_{xy}^{T_0}\frac{\partial^2 X_{m,n}}{\partial x\,\partial y}-\right.$$
$$\left.k_oX_mX_n-k_wX_mX_n+k_G\nabla^2\left(X_{m,n}\right)-A_s\left(\frac{3}{4}\frac{\partial^4 X_{m,n}}{\partial x^2\partial y^2}+\frac{1}{8}\frac{\partial^4 X_m}{\partial x^4}X_n+\frac{1}{8}\frac{\partial^4 X_n}{\partial y^4}X_m\right)\right]X_mX_n dydx$$

$$K_{45}=\int_0^{Lx}\int_0^{Ly}\left[\left(2\bar{e}_{31}V_0-N_x^{T_0}\right)\frac{\partial^2 X_m}{\partial x^2}X_n+\left(2\bar{e}_{31}V_0-N_y^{T_0}\right)\frac{\partial^2 X_n}{\partial y^2}X_m+2N_{xy}^{T_0}\frac{\partial^2 X_{m,n}}{\partial x\,\partial y}-k_oX_mX_n-k_wX_mX_n+k_G\nabla^2\left(X_{m,n}\right)\right.$$
$$\left.-A_s\left(\frac{3}{2}\frac{\partial^4 X_{m,n}}{\partial x^2\partial y^2}+\frac{1}{4}\frac{\partial^4 X_m}{\partial x^4}X_n+\frac{1}{4}\frac{\partial^4 X_n}{\partial y^4}X_m\right)\right]X_mX_n dydx$$

$$K_{46}=-E_{15}\int_0^{Lx}\int_0^{Ly}\left[\frac{\partial^2 X_m}{\partial x^2}X_n+\frac{\partial^2 X_n}{\partial y^2}X_m\right]X_mX_n dydx$$

$$K_{51}=k_o\int_0^{Lx}\int_0^{Ly}X_m^{\,2}X_n^{\,2}dydx$$

$$K_{52}=k_o\int_0^{Lx}\int_0^{Ly} X_m{}^2 X_n{}^2 dydx$$

$$K_{53}=0$$

$$K_{54}=\int_0^{Lx}\int_0^{Ly}\left[-k_o X_m X_n-k_w X_m X_n+k_G\nabla^2\left(X_{m,n}\right)+2N_{xy}^{T_0}\frac{\partial^2 X_{m,n}}{\partial x\,\partial y}+\left(2\bar{e}_{31}V_0-N_x^{T_0}\right)\frac{\partial^2 X_m}{\partial x^2}X_n+\left(2\bar{e}_{31}V_0-N_y^{T_0}\right)\frac{\partial^2 X_n}{\partial y^2}X_m-\right.$$
$$\left.A_s\left(\frac{3}{2}\frac{\partial^4 X_{m,n}}{\partial x^2\partial y^2}+\frac{1}{4}\frac{\partial^4 X_m}{\partial x^4}X_n+\frac{1}{4}\frac{\partial^4 X_n}{\partial y^4}X_m\right)\right]X_m X_n dydx$$

$$K_{55}=\int_0^{Lx}\int_0^{Ly}\left[-k_o X_m X_n-k_w X_m X_n+k_G\nabla^2\left(X_{m,n}\right)+2N_{xy}^{T_0}\frac{\partial^2 X_{m,n}}{\partial x\,\partial y}+D_{11}\frac{\partial^4 X_m}{\partial x^4}X_n+D_{22}\frac{\partial^4 X_n}{\partial y^4}X_m+\left(2D_{12}+2D_{66}\right)\frac{\partial^4 X_{m,n}}{\partial x^2\partial y^2}\right.$$
$$\left.+\left(2\bar{e}_{31}V_0-N_x^{T_0}\right)\frac{\partial^2 X_m}{\partial x^2}X_n+\left(2\bar{e}_{31}V_0-N_y^{T_0}\right)\frac{\partial^2 X_n}{\partial y^2}X_m-A_s\left(3\frac{\partial^4 X_{m,n}}{\partial x^2\partial y^2}+\frac{1}{2}\frac{\partial^4 X_m}{\partial x^4}X_n+\frac{1}{2}\frac{\partial^4 X_n}{\partial y^4}X_m\right)\right]X_m X_n dydx$$

$$K_{56}=E_{31}\int_0^{Lx}\int_0^{Ly}\left[\frac{\partial^2 X_m}{\partial x^2}X_n+\frac{\partial^2 X_n}{\partial y^2}X_m\right]X_m X_n dydx$$

$$K_{61}=K_{62}=K_{63}=0$$

$$K_{64}=E_{15}\int_0^{Lx}\int_0^{Ly}\left[\frac{\partial^2 X_m}{\partial x^2}X_n+\frac{\partial^2 X_n}{\partial y^2}X_m\right]X_m X_n dydx$$

$$K_{65}=-E_{31}\int_0^{Lx}\int_0^{Ly}\left[\frac{\partial^2 X_m}{\partial x^2}X_n+\frac{\partial^2 X_n}{\partial y^2}X_m\right]X_m X_n dydx$$

$$K_{66}=\int_0^{Lx}\int_0^{Ly}\left[X_{11}\left(\frac{\partial^2 X_m}{\partial x^2}X_n+\frac{\partial^2 X_n}{\partial y^2}X_m\right)-X_{33}X_m X_n\right]X_m X_n dydx$$

(50a-f)

So, to have a non-zero response, the determinant of $[K_{ij}]$ must be set to zero and then with solving the obtained equation, the critical buckling temperature would be harvested.

4. Results and discussions

In this section, based on the graphene sheets and nonlocal elasticity theory the accuracy and precision of the current formulation would be validated. Therefore, in order to compare the outcomes, some well-known available references are employed. Hence, Table 2 is used in which the results are verified with refs. [37-38]. The Table is given for the critical buckling temperature of single-layered graphene sheets in which FSDT and nonlocal theory of Eringen have been applied. From Table 2, a high correspondence of the results in the presented study with the results in refs. [37-38] can be seen. Due to using nonlocal FSDT in ref. [37], and nonlocal new first-order shear deformation theory (NFSDT) in ref. [38], it can be concluded that by the application of the simplified first-order deformation theory by which the shear correction factor has been removed, so, the results with a satisfying accuracy are obtained and that the values of the critical buckling temperature are a slightly lower in comparison with the nonlocal FSDT. Furthermore, it is obvious that whatever the plate sizes are bigger, the critical buckling temperature will be noticeably reduced. The lower results might be due to a longitudinal and lateral distribution considered in the present work which lead to the weaker plate; however, the value of the length scale parameter is so impressive. Another comparison has been presented by Table 3 for showing the difference between current function of temperature with

those developed from ref. [38]. As can be seen, the values of results at lower aspect ratios (β) are much more than the higher ones. These differences can be acceptable when the results of classical plate theory (CLPT) are taken into consideration. In addition, whatever the aspect ratio is getting further, the results of current thermal function would be in an excellent agreement. For further verification of thermal buckling obtained here, other comparative examples are shown in Table 4 by which non-dimensional critical buckling temperature subjected to uniform temperature in local condition is investigated. To achieve this aim, refs. [39-41] are used within which the refined plate theory (RPT), the sinusoidal shear deformation theory (SPT) and the four-variable hyperbolic plate theory (FHPT) were applied. As it is observed, by an increase in the length to thickness ratio the dimensionless critical buckling forces have become closer to the other research results. However with increasing the aspect ratio the closeness of the outcomes will be in an excellent agreement which can be noticeable.

Table 2	*E=1.06TPa, υ=0.25, h=0.34nm, μ=1.81nm², l=0.6h*, α =1.1×10⁻⁶K⁻¹, ks=5/6, N^T_{xy}=0, SSSS* [37-38]
Table 3	*E=1.06TPa, υ=0.25, h=0.34nm, μ=0 nm², l=0 nm, α =1.1×10⁻⁶K⁻¹, ks=5/6, N^T_{xy}=0, SSSS* [38]
Table 4	*E=1.06TPa, υ=0.25, Lx=Ly=10nm, h=0.34nm, μ=0nm², l=0nm, α =1.1×10⁻⁶K⁻¹, T^*= 1000αΔT, N^T_{xy}=0, SSSS* [39-41]

* The value has been freely chosen and at such a value the results were compared with the other research results. Note that the value might not be the exact value of the current model which means that such a value should be obtained in an experimental work.

Table 2. Validation of the results of critical buckling temperature for single-layered graphene sheets obtained from [37-38].

Lx (nm)	*Ly (nm)*	[37] (K)-NFSDT	[38] (K)-FSDT	Present study (K)-S-FSDT
10	10	1010.7	1013.0	1011.0
20	10	702.43	703.99	701.01
20	15	424.44	426.33	422.15
20	20	315.32	316.92	313.50
25	10	661.12	662.18	658.04
25	15	375.02	376.56	373.00
25	20	262.50	263.84	260.18
25	25	207.99	209.11	205.33
30	10	638.30	638.98	636.55
30	15	347.63	348.90	345.27
30	20	233.19	234.32	231.0
30	30	146.89	147.70	144.0

Table 3. Comparison of critical buckling temperature for single-layered graphene sheets developed from ref. [38] (The data in the Table are calculated by using Eqs. 8 and 18 in ref. [38]).

L_x / L_y	[38] (K)		Present study (K), S-FSDT
	CLPT	FSDT	
0.5	3457.4	3405.5	3390.6
1	1382.9	1374.6	1357.2
1.5	998.79	994.42	991.41
2	864.33	861.06	860.41
2.5	802.10	799.28	790.74
3	768.30	765.71	758.23
3.5	747.91	745.46	733.31
4	734.68	732.32	728.55
4.5	725.61	723.30	717.23
5	719.12	716.86	715.15
5.5	714.32	712.09	710.4
6	710.68	708.46	707.68
6.5	707.83	705.63	705.23
7	705.58	703.39	702.96

Table 4. Comparison of dimensionless critical buckling temperature for single-layered graphene sheets with refs. [39-41]

L_y / L_x	Plate theory	L_x/h				
		5	10	15	20	25
1	[39]-RPT	41.31747	11.97825	5.48623	2.00643	0.50499
	[40]-SPT	41.33314	11.97928	5.48645	2.00646	0.50502
	[41]-FHPT	41.31705	11.97825	5.48623	2.00643	0.50499
	Present, S-FSDT	40.15970	9.33687	4.09660	1.90833	0.46243
2	[39]	27.73011	7.63918	3.46061	1.25824	0.31589
	[40]	27.73639	7.63958	3.46070	1.25826	0.31591
	[41]	27.73004	7.63918	3.46061	1.25824	0.31589
	Present	26.3310	6.27304	2.76394	1.18566	0.29915
3	[39]	24.99110	6.81615	3.08138	1.11913	0.28083
	[40]	24.99608	6.81646	3.08145	1.11915	0.28085
	[41]	24.99106	6.81615	3.08138	1.11913	0.28083
	Present	23.39520	5.60301	2.4710	1.02185	0.26886

Table 5. Mechanical and Electrical properties of a piezoelectric nanoplate [14, 24]

A piezoelectric nanoplate	C_{11}=132GPa, C_{12}=71GPa, C_{13}=73GPa, C_{33}=115GPa, C_{44}=26GPa, C_{66}=30.5GPa, e_{31}=-4.1 C/m^2, e_{15}=10.5 C/m^2, e_{33}=14.1 C/m^2, κ_{11}=5.841e-9 C/V.m, κ_{33}=7.124e-9 C/V.m, λ_{11}=4.738e+5 N/m^{2}K, λ_{33}=4.529e+5 N/m^{2}K

Fig. 3a displays the changes of the length scale parameter in both SSSS and CCCC boundary conditions in the presence and absence of the elastic foundation. It can be clearly seen that in the *l=0*, the outcomes of critical buckling temperature in simple boundary condition are higher than clamped ones. However, with an increase in the length scale parameter, the trend will be steady. As a matter of fact, the outcomes demonstrate the effects of flexible boundary conditions and show that whatever the boundary conditions are more flexible, the results are further than others. Additionally, Fig. 3b shows the changes in the length scale parameter versus various EEV in CCCC. It is found that by increasing EEV, the critical buckling temperature is decreased. Using low values of EEV proves the major influence of EEV on the thermal buckling problems. This means that the use of greater EEV can ineffective the high resistance of nanoplates for occurring thermal buckling and at this situation, plates will buckle under low temperatures.

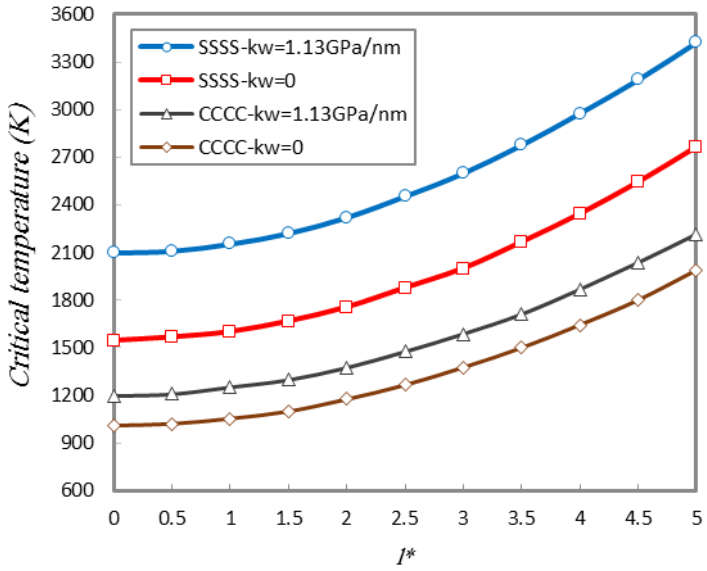

Fig. 3a. The length scale parameter versus different boundary conditions (*V_0=0 V, m=n=1, Lx=Ly=30h, l*=l/h, ko=1GPa/nm)*

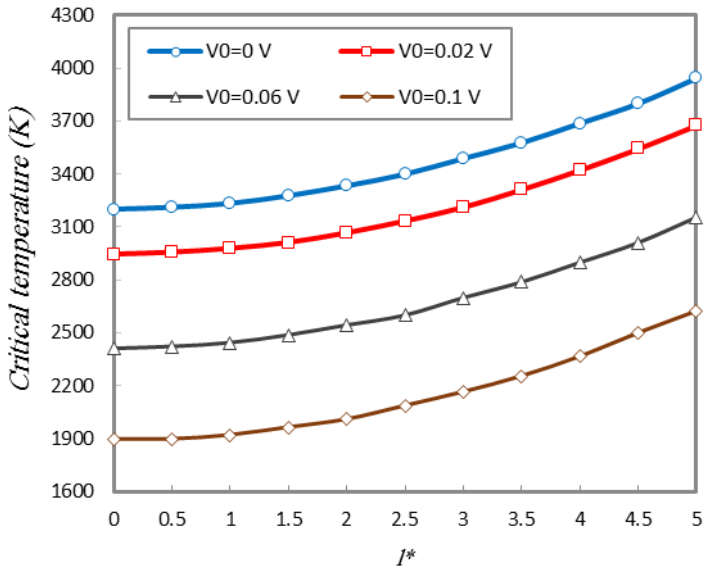

Fig. 3b. The length scale parameter versus different external electric voltage (*CCCC, m=n=1, Lx=Ly=30h, l*=l/h, ko=10GPa/nm)*

In order to examine the van der Waals (vdW) forces between layers, Fig. 4a and 4b are drawn. As shown in the Fig. 4a, by an increase in vdW forces the critical buckling temperature outputs after *ko=4GPa/nm* will be gradually converged. Before that, the slope of the diagrams tends to steeply upward. Indeed, in lower values of vdW, nanoplates have separated behaviors, and we can see asynchronous buckling in which each plate has isolated buckling. On the other hand, when the vdW forces are raised the plates will be simultaneously buckled. So, it is reasonable if we say in synchronic buckling the critical temperature must be bigger than another one [11]. Moreover, it can be observed that whatever the sizes of plates are smaller, the critical buckling temperature values will be greater. In addition, by focusing on the graph, it is vivid that the impact of the plate's dimensions is more than boundary conditions effects on the vdW differential. From the second figure which considers the vdW differential versus EEV, it can be found that the greater vdW forces have not a noticeable impressed by the EEV.

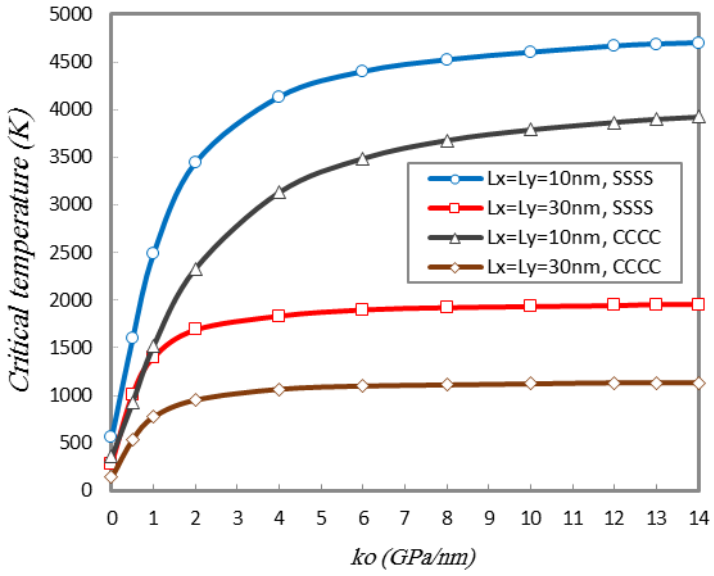

Fig. 4a. The Van der Waals coefficient versus different size of plate (V_0*=0 V, m=n=1, l=2h)*

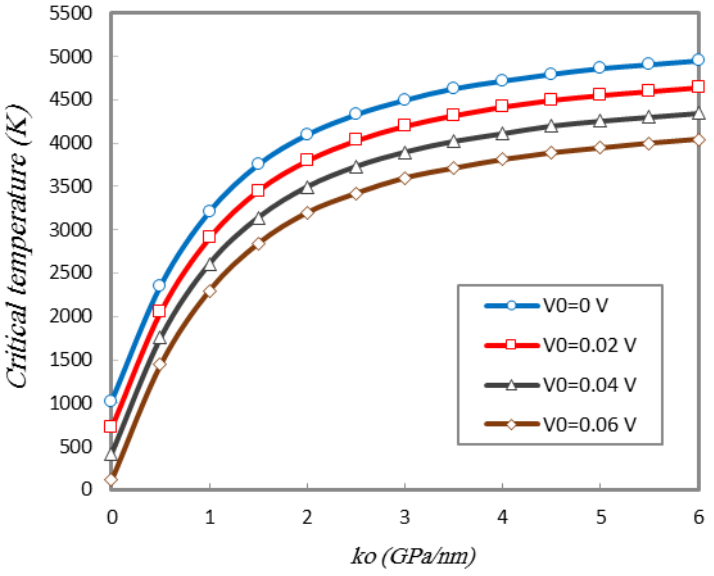

Fig. 4b. The Van der Waals coefficient versus different external electric voltage (*SSSS, Lx=Ly=30h, m=n=1, l=4h)*

Fig. 5 is plotted to show the EEV changes in the several half-waves for both CCCC and SSSS boundary conditions. As can be seen, in the first half-wave number the increase of the EEV leads to decreasing critical buckling

temperature. However, after evaluating the second half-wave number the trend is getting slower, which means that the second half-wave decreases the impact of EEV. It can be importantly noted that by investigating every boundary condition while EEV is removed, the results of CCCC in both half-waves are remarkably closer to each other against SSSS. After applying EEV on the DLPNs, EEV has a tremendous impacted on the CCCC outputs and made the far more difference between the results of half-waves. The result is seen with lesser intensity in SSSS.

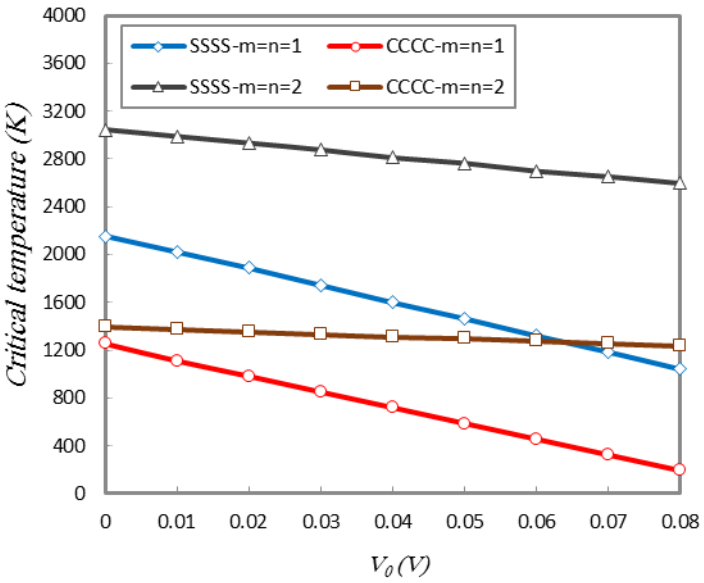

Fig. 5. The effect of different external electric voltage on different half-waves (*Lx=Ly=30h, l=h, ko=1GPa/nm*)

The several aspect ratios (β) in various EEV are illustrated in Figs. 6. Initially, Fig. 6a is shown over which L_y is constant and L_x is changeable, and also SSSS boundary condition is used. It can be clearly seen that an increase in β parameter leads to a remarkable decrease in critical buckling temperature results. In other words, the kind of distribution of temperature might be directly caused. This means that while temperature other than thickness is raised in both longitudinal and lateral dimensions, the impact of dimensions of the plate is fundamentally grown. Moreover, increasing dimensions of the plate has a considerable influence on the EEV which leads to proximity of results in various EEV. As a rule, it can be concluded that by increasing length of the plate the effects of EEV are declined. From Fig. 6b in which L_x is constant and L_y is variable the conclusion of previous figure is not seen and decreasing of the critical forces has slower trend against Fig. 6a.

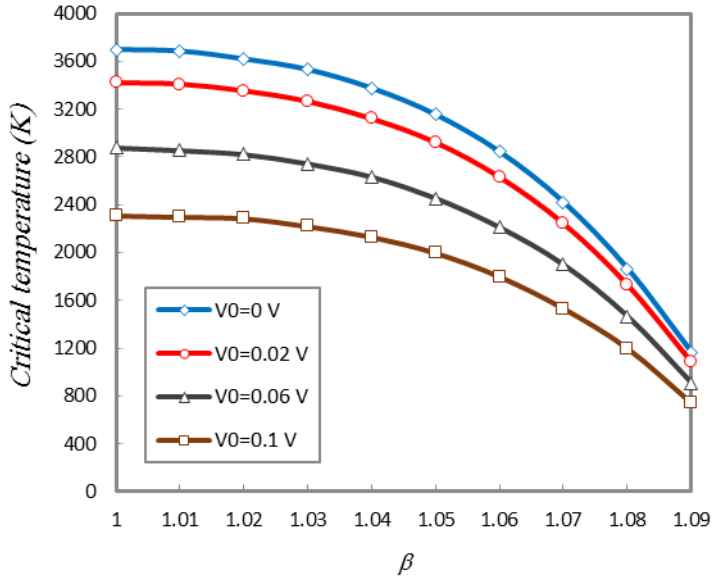

Fig. 6a. The effect of external electric voltages on aspect ratio changes (*SSSS, m=n=1, Ly=30h, l=h, ko=4GPa/nm*)

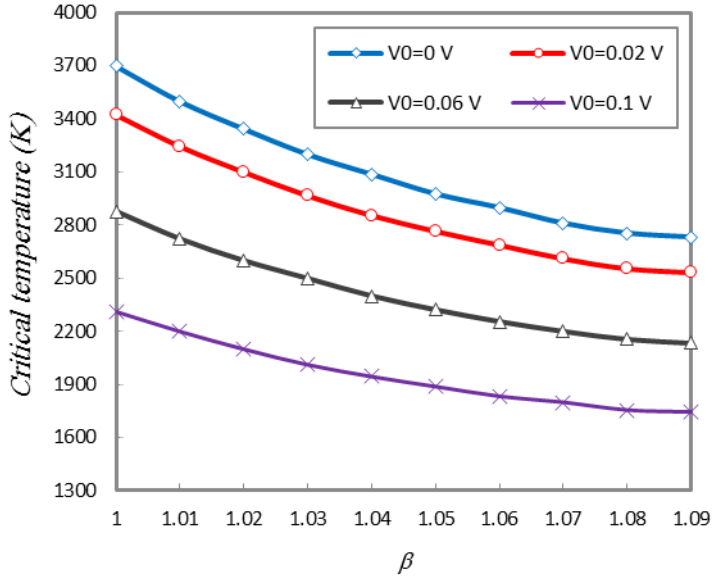

Fig. 6b. The effect of external electric voltages on aspect ratio changes (*SSSS, m=n=1, Lx=30h, l=h, ko=4GPa/nm*)

Fig. 7a studies the effects of elastic foundation on the EEV changes by taking into account simple boundary condition. It can be easily found that by increasing the strength of the matrix the critical buckling temperature has been monotonously increased. The considerable slope has been made whenever the foundation is ignored. Moreover, the elastic foundation changes do not have a significant impact on the results of any EEV. Moreover, several in-plane thermal stress resultants are shown to investigate the effects of the temperature function in various directions by changing the elastic foundation in Fig. 7b. According to the figure, the strongest condition for the DLPNs system is when N^T_{xy} is neglected and the weakest condition is when N^T_{yy} is set to zero. In other words, it can be noted that the most impressive stress resultants are $N^T_{xx} > N^T_{xy} > N^T_{yy}$, respectively.

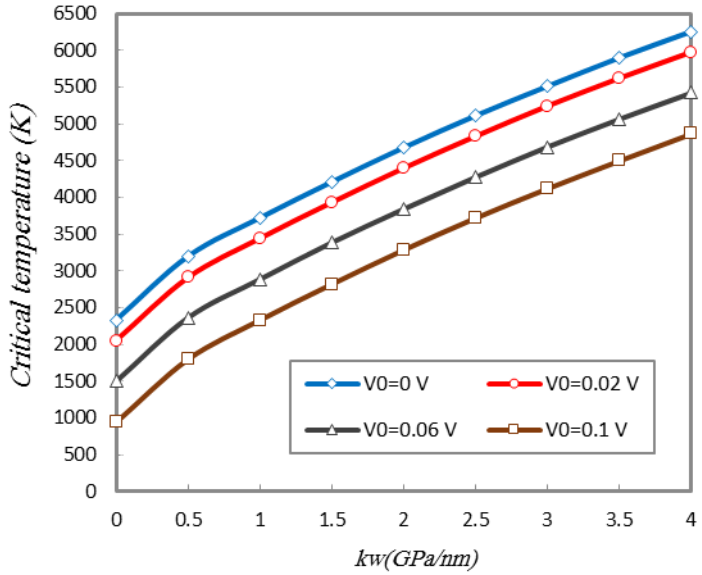

Fig. 7a. The effect of elastic foundation on external electric voltage results (*SSSS, m=n=1, Lx=Ly=30h, l=h, ko=5GPa/nm*)

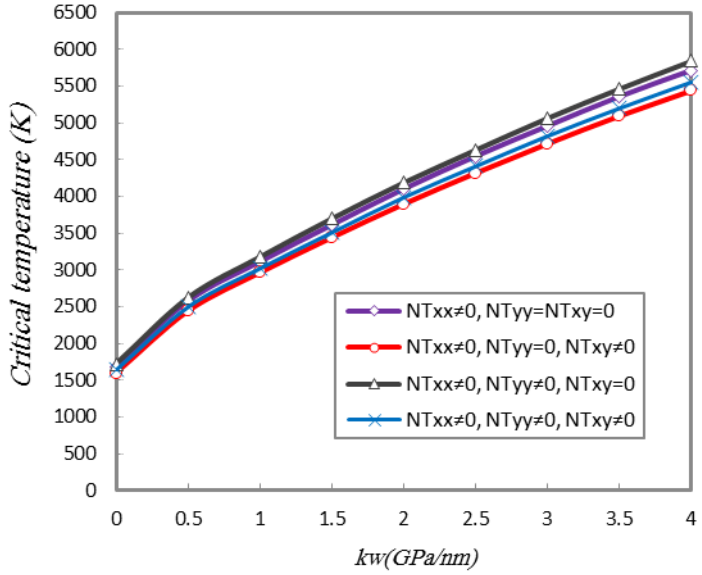

Fig. 7b. In-plane thermal stress resultants versus elastic foundation (*SSSS, V_0=0.05 V, Lx=Ly=30h, m=n=1, l=h, ko=5GPa/nm*)

6. Conclusions

This study analyzed the electro-thermal buckling of double-layered piezoelectric nanoplates under external electric voltage in the thermal environment. To achieve this aim, a simplified first-order shear deformation theory was employed to obtain the governing equations by taking into account the Von-Kármán assumption. The effect of the small-scale was investigated by using modified couple stress theory. Moreover, an analytical solution was used to extract the results by changing various parameters. In conclusion, some of the important results achieved from the present study are as follows:

- EEV has a considerable impacted on the results of various half-waves in all boundary conditions.
- By increasing EEV, the reduction of critical buckling temperature in higher half-waves is remarkably slower than lower half-waves.
- By considering long lengths, the effect of EEV on the critical temperature will be markedly decreased.

References

[1] https://www.mide.com.

[2] G. Ciofani, A. Menciassi, (2012), Piezoelectric Nanomaterials for Biomedical Applications, Nanomedicine and Nanotoxicology, ISBN 978-3-642-28044-3, 1-27, Springer-Verlag, Berlin, (2012).

[3] L. L. Ke, Y. S. Wang, Z. D. Wang, Nonlinear vibration of the piezoelectric nanobeams based on the nonlocal theory, Compos. Struct., Vol. 94 No. 6, pp. 2038–2047.

[4] C. Liu, L. L. Ke, Y. S. Wang, J. Yang, Kitipornchai S., (2014), Buckling and post-buckling of size-dependent piezoelectric Timoshenko nanobeams subject to thermo-electro-mechanical loadings, Int. J. Struct. Stab. Dyn., Vol. 14, pp. 1350067, https://doi.org/10.1142/S0219455413500673.

[5] L. Y. Jiang, Z. Yan, (2012), Vibration and buckling analysis of a piezoelectric nanoplate considering surface effects and in-plane constraints, Proc. R. Soc. A., Vol. 468, pp. 3458-3475.

[6] B. Akgöz, Ö. Civalek, (2012), Free vibration analysis for single-layered graphene sheets in an elastic matrix via modified couple stress theory, Materials and Design, Vol. 42, pp. 164–171.

[7] Ch. Chen, Sh. Li, L. Dai, C-Z Qian, (2014), Buckling and stability analysis of a piezoelectric viscoelastic nanobeam subjected to van der Waals forces, Commun. Nonlinear Sci. Numer. Simulat., Vol. 19, pp. 1626–1637.

[8] K. F. Wang, T. Kitamura, B. Wang, (2015), Nonlinear pull-in instability and free vibration of micro/nanoscale plates with surface energy-a modified couple stress theory model, Int. J of Mech. Sci., Vol. 99, pp. 288-296.

[9] M. Akbarzadeh Khorshidi, M. Shariati, S. A. Emam, (2016), Postbuckling of functionally graded nanobeams based on modified couple stress theory under general beam theory, Int. J of Mech. Sci., Vol. 110 No. 4, pp. 160-169.

[10] J. Lou, L. He, J. Du, H. Wu, (2016), Buckling and post-buckling analyses of piezoelectric hybrid microplates subject to thermo-electro-mechanical loads based on the modified couple stress theory, Compos. Struct., Vol. 153, pp. 332-344.

[11] M. Malikan, M. Jabbarzadeh, Sh. Dastjerdi, (2017), Non-linear Static stability of bi-layer carbon nanosheets resting on an elastic matrix under various types of in-plane shearing loads in thermo-elasticity using nonlocal continuum, Microsyst. Technol., Vol. 23 No. 7, pp. 2973–2991.

[12] M. Habibnejad Korayem, A. Habibnejad Korayem, (2017), Studied modeling of AFM with a piezoelectric layer based on the modified couple stress theory with geometric discontinuities, Appl. Math. Model., Vol. 45, pp. 439–456.

[13] J. Guo, J. Chen, E. Pan, (2017), Free vibration of three-dimensional anisotropic layered composite nanoplates based on modified couple-stress theory, Physica E: Low-dimensional Systems and Nanostructures, Vol. 87, pp. 98–106.

[14] M. Malikan, (2017), Electro-mechanical shear buckling of piezoelectric nanoplate using modified couple stress theory based on simplified first order shear deformation theory, Appl. Math. Model., Vol. 48, pp. 196–207.

[15] A. Al-Rub, R. Kamel, (2004), Material length scales in gradient-dependent plasticity/damage and size effects: theory and computation, LSU Doctoral Dissertations. 3054.
http://digitalcommons.lsu.edu/gradschool_dissertations/3054

[16] R. D. Mindlin, N. N. Eshel, (1968), On first strain-gradient theories in linear elasticity, Int. J. of Solids and Struc., Vol. 4 No. 1, pp. 109-124.

[17] R. A. Toupin, (1962), Elastic materials with couple stresses, Archive for Rational Mechanics and Analysis, Vol. 11 No. 1, pp. 385-414.

[18] R. A. Toupin, (1964), Theories of elasticity with couple-stress, Archive for Rational Mechanics and Analysis, Vol. 17 No. 2, pp. 85-112.

[19] R. D. Mindlin, H. F. Tiersten, (1962), Effects of couple-stresses in linear elasticity, Archive for Rational Mechanics and Analysis, Vol. 11 No. 1, pp. 415-448.

[20] W. T. Koiter, (1964), Couple stresses in the theory of elasticity, I and II. Proc K Ned Akad Wet (B), Vol. 67 No. 1, pp. 17–44.

[21] E. Cosserat, F. Cosserat, (1909), Theory of deformable bodies. In: Delphenich DH, editor. Scientific Library, 6. Paris: A. Herman and Sons, Sorbonne 6.

[22] F. Yang, A. C. M. Chong, D. C. C. Lam, P. Tong, (2002), Couple stress based strain gradient theory for elasticity, Int. J. Solids and Struct., Vol. 39 No. 10, pp. 2731–43.

[23] B. Akgöz, Ö. Civalek, (2013), A size-dependent shear deformation beam model based on the strain gradient elasticity theory, Int. J. Eng. Sci., Vol. 70, pp. 1–14.

[24] H. T. Thai, P. V. Thuc, T. K. Nguyen, J. Lee, (2015), Size-dependent behavior of functionally graded sandwich microbeams based on the modified couple stress theory, Compos. Struct., Vol. 123, pp. 337–349.

[25] C. Liu, L. L. Ke, J. Yang, S. Kitipornchai, Y. S. Wang, (2016), Buckling and post-buckling analysis of size-dependent piezoelectric nanoplates, Theo. & Appl. Mech. Lett., Vol. 6 No. 6, pp. 253-267.

[26] M. Malikan, (2017), Analytical predictions for buckling of a nanoplate subjected to nonuniform compression based on four-variable plate theory, Journal of Applied and Computational Mechanics, Vol. 3 No. 3, pp. 218–228.

[27] M. Malikan, (2018), Buckling analysis of a micro composite plate with nano coating based on the modified couple stress theory, Journal of Applied and Computational Mechanics, Vol. 4, No. 1, pp. 1–15.

[28] M. Malikan, (2018), Temperature influences on shear stability of a nanosize plate with piezoelectricity effect, Multidiscipline modeling in materials and structures, Vol. 14 No. 1, pp. 125-142.

[29] A. C. Eringen, (2002), Nonlocal continuum field theories, Springer, New York.

[30] L. L. Ke, C. Liu, Y. S. Wang, (2015), Free vibration of nonlocal piezoelectric nanoplates under various boundary conditions, Physica E: Low-dimensional Systems and Nanostructures, Vol. 66, pp. 93–106.

[31] Q. Wang, (2002), Axi-symmetric wave propagation in a cylinder coated with a piezoelectric layer, Int. J. Solids and Struct., Vol. 39 No. 11, pp. 3023–3037.

[32] M. L. Gossard, P. Seide, W. M. Roberts, (1952), Thermal buckling of plates, NACA TN 2771, United States. National Advisory Committee for Aeronautics.

[33] Heldenfels, R. R. Roberts, M. William, (1952), Experimental and theoretical determination of thermal stresses in a flat plate. NACA TN 2769, United States.

[34] M. R. Barati, M. H. Sadr, A. M. Zenkour, (2016), Buckling analysis of higher order graded smart piezoelectric plates with porosities resting on elastic foundation, Int. J of Mech. Sci., Vol. 117, pp. 309-320.

[35] A. Doroushi, M. R. Eslami, A. Komeili, (2011), Vibration analysis and transient response of an FGPM beam under thermo-electro-mechanical loads using higher-order shear deformation theory, Journal of Intelligent Material Systems and Structures, Vol. 22 No. 3, pp. 231-243.

[36] P. A. Jadhav, K. M. Bajoria, (2013), Free and forced vibration control of piezoelectric FGM plate subjected to electro-mechanical loading, Smart Materials and Structures, Vol. 22 No. 6, pp. 065021.

[37] N. Radic, D. Jeremić, (2016), Thermal buckling of double-layered graphene sheets embedded in an elastic medium with various boundary conditions using a nonlocal new first-order shear deformation theory, Composites: Part B, Vol. 97, pp. 201–215.

[38] Y. Z. Wang, H. T. Cui, F. M. Li, K. Kishimoto, (2013), Thermal buckling of a nanoplate with small-scale effects, Acta Mech., Vol. 224 No. 6, pp. 1299-1307.

[39] M. Bouazza, T. Becheri, A. Boucheta, N. Benseddiq, (2016), Thermal buckling analysis of nanoplates based on nonlocal elasticity theory with four-unknown shear deformation theory resting on Winkler–Pasternak elastic foundation, Int. J. Comput. Methods Eng. Sci. Mech., Vol. 17 No. 5-6, pp. 362–373.

[40] A. M. Zenkour, M. Sobhy, (2013), Nonlocal elasticity theory for thermal buckling of nanoplates lying on Winkler–Pasternak elastic substrate medium, Physica E: Low-dimensional Systems and Nanostructures, Vol. 53, pp. 251–259.

[41] M. Bouazza, A. M. Zenkour, N. Benseddiq, (2018), Closed-from solutions for thermal buckling analyses of advanced nanoplates according to a hyperbolic four-variable refined theory with small-scale effects, Acta Mech., DOI: https://doi.org/10.1007/s00707-017-2097-8.